

# The Finite Element Method in Geodynamics

C. Thieulot

December 28, 2018

## Contents

<b>1</b>	<b>Introduction</b>	<b>4</b>
1.1	Acknowledgments . . . . .	4
1.2	Essential literature . . . . .	4
1.3	Installation . . . . .	4
<b>2</b>	<b>The physical equations of Fluid Dynamics</b>	<b>5</b>
2.1	the Boussinesq approximation: an Incompressible flow . . . . .	8
<b>3</b>	<b>The Finite Element Method</b>	<b>9</b>
3.1	Numerical integration . . . . .	9
3.1.1	in 1D - theory . . . . .	9
3.1.2	in 1D - examples . . . . .	11
3.1.3	in 2D/3D - theory . . . . .	11
3.2	The mesh . . . . .	12
3.3	Elements and basis functions in 1D . . . . .	12
3.4	Elements and basis functions in 2D . . . . .	12
3.4.1	The $Q_1$ basis in 2D . . . . .	13
3.4.2	The $Q_2$ basis in 2D . . . . .	14
3.5	The penalty approach . . . . .	14
<b>4</b>	<b>Additional techniques</b>	<b>18</b>
4.1	The method of manufactured solutions . . . . .	18
4.2	Sparse storage . . . . .	18
4.3	Mesh generation . . . . .	18
4.4	The value of the timestep . . . . .	18
4.5	Tracking materials . . . . .	18
4.6	Visco-Plasticity . . . . .	18
4.7	Picard and Newton . . . . .	18
4.8	The choice of solvers . . . . .	18
4.9	The SUPG formulation for the energy equation . . . . .	18
4.10	Tracking materials and/or interfaces . . . . .	18
4.11	Dealing with a free surface . . . . .	18
4.12	Pressure normalisation . . . . .	18
<b>5</b>	<b>fieldstone: simple analytical solution</b>	<b>20</b>
<b>6</b>	<b>fieldstone: Stokes sphere</b>	<b>23</b>
<b>7</b>	<b>fieldstone: Convection in a 2D box</b>	<b>24</b>
<b>8</b>	<b>fieldstone: solcx benchmark</b>	<b>26</b>
<b>9</b>	<b>fieldstone: solkz benchmark</b>	<b>28</b>
<b>10</b>	<b>fieldstone: solvi benchmark</b>	<b>29</b>
<b>11</b>	<b>fieldstone: the indentor benchmark</b>	<b>31</b>
<b>12</b>	<b>fieldstone: the annulus benchmark</b>	<b>33</b>

13 fieldstone: stokes sphere (3D) - penalty	35
14 fieldstone: stokes sphere (3D) - mixed formulation	36
15 fieldstone: consistent pressure recovery	37
16 fieldstone: the Particle in Cell technique (1) - the effect of averaging	38
17 fieldstone: solving the full saddle point problem	41
18 fieldstone: solving the full saddle point problem in 3D	43
19 fieldstone: solving the full saddle point problem with $Q_2 \times Q_1$ elements	46
20 fieldstone: The non-conforming $Q_1 \times P_0$ element	48
21 fieldstone: The stabilised $Q_1 \times Q_1$ element	49
22 fieldstone: compressible flow (1)	50
<b>23 fieldstone: compressible flow (2)</b>	<b>52</b>
23.1 The physics . . . . .	52
23.2 The numerics . . . . .	52
23.3 The experimental setup . . . . .	53
23.4 Scaling . . . . .	54
23.5 Conservation of energy 1 . . . . .	54
23.5.1 under BA and EBA approximations . . . . .	54
23.5.2 under no approximation at all . . . . .	55
23.6 Conservation of energy 2 . . . . .	55
23.7 The problem of the onset of convection . . . . .	56
23.8 results - BA - $Ra = 10^4$ . . . . .	58
23.9 results - BA - $Ra = 10^5$ . . . . .	60
23.10 results - BA - $Ra = 10^6$ . . . . .	61
23.11 results - EBA - $Ra = 10^4$ . . . . .	62
23.12 results - EBA - $Ra = 10^5$ . . . . .	64
23.13 Onset of convection . . . . .	65
<b>A The main codes in computational geodynamics</b>	<b>66</b>
A.1 ADELI . . . . .	66
A.2 ASPECT . . . . .	66
A.3 CITCOMS and CITCOMCU . . . . .	66
A.4 DOUAR . . . . .	66
A.5 GAIA . . . . .	66
A.6 GALE . . . . .	66
A.7 GTECTON . . . . .	66
A.8 ELVIS . . . . .	66
A.9 ELEFANT . . . . .	66
A.10 ELLIPSIS . . . . .	66
A.11 FANTOM . . . . .	66
A.12 FLUIDITY . . . . .	66
A.13 LAMEM . . . . .	66
A.14 MILAMIN . . . . .	66
A.15 PARAVOZ/FLAMAR . . . . .	66
A.16 PTATIN . . . . .	66
A.17 RHEA . . . . .	66
A.18 SEPRAN . . . . .	66
A.19 SOPALE . . . . .	66
A.20 STAGYY . . . . .	66
A.21 SULEC . . . . .	66
A.22 TERRA . . . . .	66
A.23 UNDERWORLD 1&2 . . . . .	66

B	fieldstone.py	67
C	fieldstone_stokes_sphere.py	68
D	fieldstone_convection_box.py	68
E	fieldstone_solcx.py	69
F	fieldstone_indentor.py	70
G	fieldstone_saddlepoint.py	71

# 1 Introduction

## WARNING: this is work in progress

practical hands-on approach

as little as possible jargon

no mathematical proof

no optimised codes (readability over efficiency). avoiding as much as possible to have to look elsewhere. very sequential, so unavoidable repetitions (jacobian, shape functions)

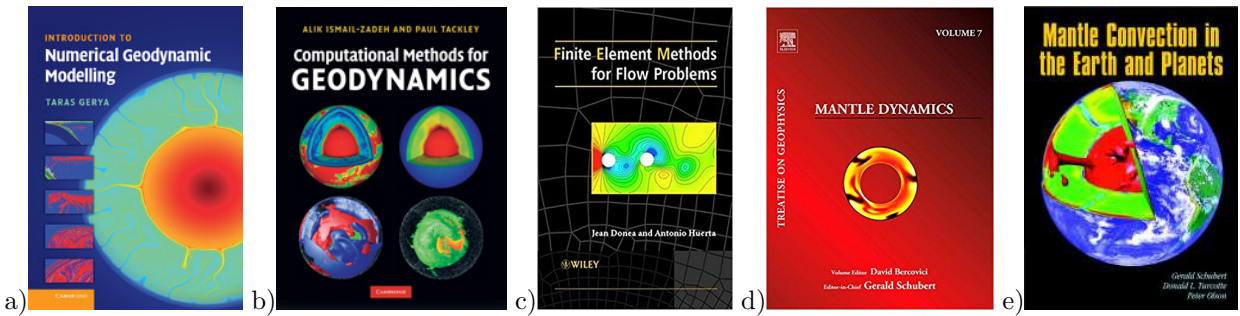
FE is one of several methods.

All the python scripts and this document are freely available at <https://github.com/cedrict/fieldstone>.

### 1.1 Acknowledgments

Jean Braun, Philippe Fullsack, Arie van den Berg, Lukas van de Wiel, Robert Myhill, Menno, Anne Too many BSc and MSc students to name individually, although Job Mos did produce the very first version of fieldstone as part of his MSc thesis. The ASPECT team in general and Wolfgang Bangerth and Timo Heister in particular.

### 1.2 Essential literature



### 1.3 Installation

```
python3.6 -m pip install --user numpy scipy matplotlib
```

## 2 The physical equations of Fluid Dynamics

Symbol	meaning	unit
$t$	Time	s
$x, y, z$	Cartesian coordinates	m
$\mathbf{v}$	velocity vector	$\text{m} \cdot \text{s}^{-1}$
$\rho$	mass density	$\text{kg/m}^3$
$\eta$	dynamic viscosity	$\text{Pa} \cdot \text{s}$
$\lambda$	penalty parameter	$\text{Pa} \cdot \text{s}$
$T$	temperature	K
$\nabla$	gradient operator	$\text{m}^{-1}$
$\nabla \cdot$	divergence operator	$\text{m}^{-1}$
$p$	pressure	Pa
$\dot{\epsilon}(\mathbf{v})$	strain rate tensor	$\text{s}^{-1}$
$\alpha$	thermal expansion coefficient	$\text{K}^{-1}$
$k$	thermal conductivity	$\text{W}/(\text{m} \cdot \text{K})$
$C_p$	Heat capacity	J/K
$H$	intrinsic specific heat production	$\text{W/kg}$
$\beta_T$	isothermal compressibility	$\text{Pa}^{-1}$

Let us start from the heat transport equation as shown in Schubert, Turcotte and Olson [47]:

$$\rho C_p \frac{DT}{Dt} - \alpha T \frac{Dp}{Dt} = \nabla \cdot k \nabla T + \Phi + \rho H$$

with

$$\frac{DT}{Dt} = \frac{\partial T}{\partial t} + \mathbf{v} \cdot \nabla T \quad \frac{Dp}{Dt} = \frac{\partial p}{\partial t} + \mathbf{v} \cdot \nabla p$$

In order to arrive at the set of equations that ASPECT solves, we need to neglect the  $\partial p / \partial t$ . **WHY?** Also, their definition of the shear heating term  $\Phi$  is:

$$\Phi = k_B (\nabla \cdot \mathbf{v})^2 + 2\eta \dot{\epsilon}^d : \dot{\epsilon}^d$$

For many fluids the bulk viscosity  $k_B$  is very small and is often taken to be zero, an assumption known as the Stokes assumption:  $k_B = \lambda + 2\eta/3 = 0$ . Note that  $\eta$  is the dynamic viscosity and  $\lambda$  the second viscosity. Also,

$$\boldsymbol{\tau} = 2\eta \dot{\epsilon} + \lambda (\nabla \cdot \mathbf{v}) \mathbf{1}$$

but since  $k_B = \lambda + 2\eta/3 = 0$ , then  $\lambda = -2\eta/3$  so

$$\boldsymbol{\tau} = 2\eta \dot{\epsilon} - \frac{2}{3}\eta (\nabla \cdot \mathbf{v}) \mathbf{1} = 2\eta \dot{\epsilon}^d$$

[from aspect manual] We focus on the system of equations in a  $d = 2$ - or  $d = 3$ -dimensional domain  $\Omega$  that describes the motion of a highly viscous fluid driven by differences in the gravitational force due to a density that depends on the temperature. In the following, we largely follow the exposition of this material in Schubert, Turcotte and Olson [47].

Specifically, we consider the following set of equations for velocity  $\mathbf{u}$ , pressure  $p$  and temperature  $T$ :

$$-\nabla \cdot \left[ 2\eta \left( \dot{\epsilon}(\mathbf{v}) - \frac{1}{3}(\nabla \cdot \mathbf{v}) \mathbf{1} \right) \right] + \nabla p = \rho \mathbf{g} \quad \text{in } \Omega, \quad (1)$$

$$\nabla \cdot (\rho \mathbf{v}) = 0 \quad \text{in } \Omega, \quad (2)$$

$$\begin{aligned} \rho C_p \left( \frac{\partial T}{\partial t} + \mathbf{v} \cdot \nabla T \right) - \nabla \cdot k \nabla T &= \rho H \\ &+ 2\eta \left( \dot{\epsilon}(\mathbf{v}) - \frac{1}{3}(\nabla \cdot \mathbf{v}) \mathbf{1} \right) : \left( \dot{\epsilon}(\mathbf{v}) - \frac{1}{3}(\nabla \cdot \mathbf{v}) \mathbf{1} \right) \\ &+ \alpha T (\mathbf{v} \cdot \nabla p) \\ &+ \rho T \Delta S \left( \frac{\partial X}{\partial t} + \mathbf{v} \cdot \nabla X \right) \end{aligned} \quad \text{in } \Omega, \quad (3)$$

where  $\dot{\epsilon}(\mathbf{u}) = \frac{1}{2}(\nabla \mathbf{u} + \nabla \mathbf{u}^T)$  is the symmetric gradient of the velocity (often called the *strain rate*).

In this set of equations, (87) and (88) represent the compressible Stokes equations in which  $\mathbf{v} = \mathbf{v}(\mathbf{x}, t)$  is the velocity field and  $p = p(\mathbf{x}, t)$  the pressure field. Both fields depend on space  $\mathbf{x}$  and time  $t$ . Fluid flow is driven by the gravity force that acts on the fluid and that is proportional to both the density of the fluid and the strength of the gravitational pull.

Coupled to this Stokes system is equation (89) for the temperature field  $T = T(\mathbf{x}, t)$  that contains heat conduction terms as well as advection with the flow velocity  $\mathbf{v}$ . The right hand side terms of this equation correspond to

- internal heat production for example due to radioactive decay;
- friction (shear) heating;
- adiabatic compression of material;
- phase change.

The last term of the temperature equation corresponds to the latent heat generated or consumed in the process of phase change of material. In what follows we will not assume that no phase change takes place so that we disregard this term altogether.

A note on the shear heating term  $\Phi$ : In many publications,  $\Phi$  is given by  $\Phi = \tau_{ij}\partial_j u_i = \boldsymbol{\tau} : \nabla \mathbf{v}$ .

$$\Phi = \tau_{ij}\partial_j u_i \quad (4)$$

$$= 2\eta \dot{\epsilon}_{ij}^d \partial_j u_i \quad (5)$$

$$= 2\eta \frac{1}{2} (\dot{\epsilon}_{ij}^d \partial_j u_i + \dot{\epsilon}_{ji}^d \partial_i u_j) \quad (6)$$

$$= 2\eta \frac{1}{2} (\dot{\epsilon}_{ij}^d \partial_j u_i + \dot{\epsilon}_{ij}^d \partial_i u_j) \quad (7)$$

$$= 2\eta \dot{\epsilon}_{ij}^d \frac{1}{2} (\partial_j u_i + \partial_i u_j) \quad (8)$$

$$= 2\eta \dot{\epsilon}_{ij}^d \dot{\epsilon}_{ij} \quad (9)$$

$$= 2\eta \dot{\boldsymbol{\epsilon}}^d : \dot{\boldsymbol{\epsilon}} \quad (10)$$

$$= 2\eta \dot{\boldsymbol{\epsilon}}^d : \left( \dot{\boldsymbol{\epsilon}}^d + \frac{1}{3}(\nabla \cdot \mathbf{v})\mathbf{1} \right) \quad (11)$$

$$= 2\eta \dot{\boldsymbol{\epsilon}}^d : \dot{\boldsymbol{\epsilon}}^d + 2\eta \dot{\boldsymbol{\epsilon}}^d : \mathbf{1}(\nabla \cdot \mathbf{v}) \quad (12)$$

$$= 2\eta \dot{\boldsymbol{\epsilon}}^d : \dot{\boldsymbol{\epsilon}}^d \quad (13)$$

Finally

$$\Phi = \boldsymbol{\tau} : \nabla \mathbf{v} = 2\eta \dot{\boldsymbol{\epsilon}}^d : \dot{\boldsymbol{\epsilon}}^d = 2\eta ((\dot{\epsilon}_{xx}^d)^2 + (\dot{\epsilon}_{yy}^d)^2 + 2(\dot{\epsilon}_{xy}^d)^2)$$

## 2.1 the Boussinesq approximation: an Incompressible flow

[from aspect manual] The Boussinesq approximation assumes that the density can be considered constant in all occurrences in the equations with the exception of the buoyancy term on the right hand side of (87). The primary result of this assumption is that the continuity equation (88) will now read

$$\nabla \cdot \mathbf{v} = 0$$

This implies that the strain rate tensor is deviatoric. Under the Boussinesq approximation, the equations are much simplified:

$$-\nabla \cdot [2\eta\dot{\epsilon}(\mathbf{v})] + \nabla p = \rho\mathbf{g} \quad \text{in } \Omega, \quad (14)$$

$$\nabla \cdot (\rho\mathbf{v}) = 0 \quad \text{in } \Omega, \quad (15)$$

$$\rho_0 C_p \left( \frac{\partial T}{\partial t} + \mathbf{v} \cdot \nabla T \right) - \nabla \cdot k \nabla T = \rho H \quad \text{in } \Omega \quad (16)$$

Note that all terms on the rhs of the temperature equations have disappeared, with the exception of the source term.

### 3 The Finite Element Method

#### 3.1 Numerical integration

As we will see later, using the Finite Element method to solve problems involves computing integrals which are more often than not too complex to be computed analytically/exactly. We will then need to compute them numerically.

[wiki] In essence, the basic problem in numerical integration is to compute an approximate solution to a definite integral

$$\int_a^b f(x)dx$$

to a given degree of accuracy. This problem has been widely studied [?] and we know that if  $f(x)$  is a smooth function, and the domain of integration is bounded, there are many methods for approximating the integral to the desired precision.

There are several reasons for carrying out numerical integration.

- The integrand  $f(x)$  may be known only at certain points, such as obtained by sampling. Some embedded systems and other computer applications may need numerical integration for this reason.
- A formula for the integrand may be known, but it may be difficult or impossible to find an antiderivative that is an elementary function. An example of such an integrand is  $f(x) = \exp(-x^2)$ , the antiderivative of which (the error function, times a constant) cannot be written in elementary form.
- It may be possible to find an antiderivative symbolically, but it may be easier to compute a numerical approximation than to compute the antiderivative. That may be the case if the antiderivative is given as an infinite series or product, or if its evaluation requires a special function that is not available.

##### 3.1.1 in 1D - theory

The simplest method of this type is to let the interpolating function be a constant function (a polynomial of degree zero) that passes through the point  $((a + b)/2, f((a + b)/2))$ .

This is called the midpoint rule or rectangle rule.

$$\int_a^b f(x)dx \simeq (b - a)f\left(\frac{a + b}{2}\right)$$

insert here figure

The interpolating function may be a straight line (an affine function, i.e. a polynomial of degree 1) passing through the points  $(a, f(a))$  and  $(b, f(b))$ .

This is called the trapezoidal rule.

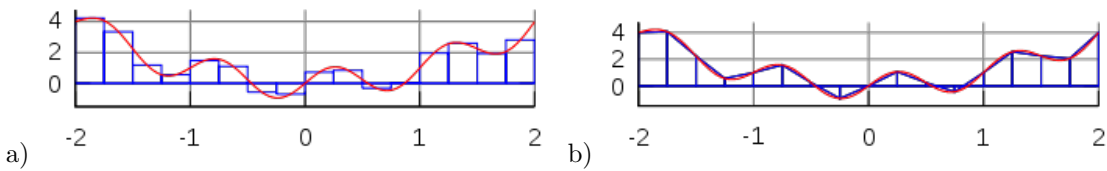
$$\int_a^b f(x)dx \simeq (b - a)\frac{f(a) + f(b)}{2}$$

insert here figure

For either one of these rules, we can make a more accurate approximation by breaking up the interval  $[a, b]$  into some number  $n$  of subintervals, computing an approximation for each subinterval, then adding up all the results. This is called a composite rule, extended rule, or iterated rule. For example, the composite trapezoidal rule can be stated as

$$\int_a^b f(x)dx \simeq \frac{b - a}{n} \left( \frac{f(a)}{2} + \sum_{k=1}^{n-1} f(a + k\frac{b-a}{n}) + \frac{f(b)}{2} \right)$$

where the subintervals have the form  $[kh, (k + 1)h]$ , with  $h = (b - a)/n$  and  $k = 0, 1, 2, \dots, n - 1$ .



The interval  $[-2, 2]$  is broken into 16 sub-intervals. The blue lines correspond to the approximation of the red curve by means of a) the midpoint rule, b) the trapezoidal rule.

There are several algorithms for numerical integration (also commonly called 'numerical quadrature', or simply 'quadrature') . Interpolation with polynomials evaluated at equally spaced points in  $[a, b]$  yields the NewtonCotes formulas, of which the rectangle rule and the trapezoidal rule are examples. If we allow the intervals between interpolation points to vary, we find another group of quadrature formulas, such as the Gauss(ian) quadrature formulas. A Gaussian quadrature rule is typically more accurate than a NewtonCotes rule, which requires the same number of function evaluations, if the integrand is smooth (i.e., if it is sufficiently differentiable).

An  $n$ -point Gaussian quadrature rule, named after Carl Friedrich Gauss, is a quadrature rule constructed to yield an exact result for polynomials of degree  $2n - 1$  or less by a suitable choice of the points  $x_i$  and weights  $w_i$  for  $i = 1, \dots, n$ .

The domain of integration for such a rule is conventionally taken as  $[-1, 1]$ , so the rule is stated as

$$\int_{-1}^{+1} f(x) dx = \sum_{i_q=1}^n w_{i_q} f(x_{i_q})$$

In this formula the  $x_{i_q}$  coordinate is the  $i$ -th root of the Legendre polynomial  $P_n(x)$ .

It is important to note that a Gaussian quadrature will only produce good results if the function  $f(x)$  is well approximated by a polynomial function within the range  $[-1, 1]$ . As a consequence, the method is not, for example, suitable for functions with singularities.

Number of points, $n$	Points, $x_i$	Weights, $w_i$
1	0	2
2	$\pm\sqrt{\frac{1}{3}}$	1
3	0	$\frac{8}{9}$
	$\pm\sqrt{\frac{3}{5}}$	$\frac{5}{9}$
4	$\pm\sqrt{\frac{3}{7} - \frac{2}{7}\sqrt{\frac{6}{5}}}$	$\frac{18+\sqrt{30}}{36}$
	$\pm\sqrt{\frac{3}{7} + \frac{2}{7}\sqrt{\frac{6}{5}}}$	$\frac{18-\sqrt{30}}{36}$
5	0	$\frac{128}{225}$
	$\pm\frac{1}{3}\sqrt{5 - 2\sqrt{\frac{10}{7}}}$	$\frac{322+13\sqrt{70}}{900}$
	$\pm\frac{1}{3}\sqrt{5 + 2\sqrt{\frac{10}{7}}}$	$\frac{322-13\sqrt{70}}{900}$

Gauss-Legendre points and their weights.

As shown in the above table, it can be shown that the weight values must fulfill the following condition:

$$\sum_{i_q} w_{i_q} = 2 \tag{17}$$

and it is worth noting that all quadrature point coordinates are symmetrical around the origin.

Since most quadrature formula are only valid on a specific interval, we now must address the problem of their use outside of such intervals. The solution turns out to be quite simple: one must carry out a change of variables from the interval  $[a, b]$  to  $[-1, 1]$ .

We then consider the reduced coordinate  $r \in [-1, 1]$  such that

$$r = \frac{2}{b-a}(x-a) - 1$$

This relationship can be reversed such that when  $r$  is known, its equivalent coordinate  $x \in [a, b]$  can be computed:

$$x = \frac{b-a}{2}(1+r) + a$$

From this it follows that

$$dx = \frac{b-a}{2}dr$$

and then

$$\int_a^b f(x) dx = \frac{b-a}{2} \int_{-1}^{+1} f(r) dr \simeq \frac{b-a}{2} \sum_{i_q=1}^n w_{i_q} f(r_{i_q})$$

### 3.1.2 in 1D - examples

**example 1** Since we know how to carry out any required change of variables, we choose for simplicity  $a = -1$ ,  $b = +1$ . Let us take for example  $f(x) = \pi$ . Then we can compute the integral of this function over the interval  $[a, b]$  exactly:

$$I = \int_{-1}^{+1} f(x)dx = \pi \int_{-1}^{+1} dx = 2\pi$$

We can now use a Gauss-Legendre formula to compute this same integral:

$$I_{gq} = \int_{-1}^{+1} f(x)dx = \sum_{i_q=1}^{n_q} w_{i_q} f(x_{i_q}) = \sum_{i_q=1}^{n_q} w_{i_q} \pi = \pi \underbrace{\sum_{i_q=1}^{n_q} w_{i_q}}_{=2} = 2\pi$$

where we have used the property of the weight values of Eq.(17). Since the actual number of points was never specified, this result is valid for all quadrature rules.

**example 2** Let us now take  $f(x) = mx + p$  and repeat the same exercise:

$$I = \int_{-1}^{+1} f(x)dx = \int_{-1}^{+1} (mx + p)dx = [\frac{1}{2}mx^2 + px]_{-1}^{+1} = 2p$$

$$I_{gq} = \int_{-1}^{+1} f(x)dx = \sum_{i_q=1}^{n_q} w_{i_q} f(x_{i_q}) = \sum_{i_q=1}^{n_q} w_{i_q} (mx_{i_q} + p) = m \underbrace{\sum_{i_q=1}^{n_q} w_{i_q} x_{i_q}}_{=0} + p \underbrace{\sum_{i_q=1}^{n_q} w_{i_q}}_{=2} = 2p$$

since the quadrature points are symmetric w.r.t. to zero on the x-axis. Once again the quadrature is able to compute the exact value of this integral: this makes sense since an  $n$ -point rule exactly integrates a  $2n - 1$  order polynomial such that a 1 point quadrature exactly integrates a first order polynomial like the one above.

**example 3** Let us now take  $f(x) = x^2$ . We have

$$I = \int_{-1}^{+1} f(x)dx = \int_{-1}^{+1} x^2 dx = [\frac{1}{3}x^3]_{-1}^{+1} = \frac{2}{3}$$

and

$$I_{gq} = \int_{-1}^{+1} f(x)dx = \sum_{i_q=1}^{n_q} w_{i_q} f(x_{i_q}) = \sum_{i_q=1}^{n_q} w_{i_q} x_{i_q}^2$$

- $n_q = 1$ :  $x_{i_q}^{(1)} = 0$ ,  $w_{i_q} = 2$ .  $I_{gq} = 0$
- $n_q = 2$ :  $x_q^{(1)} = -1/\sqrt{3}$ ,  $x_q^{(2)} = 1/\sqrt{3}$ ,  $w_q^{(1)} = w_q^{(2)} = 1$ .  $I_{gq} = \frac{2}{3}$
- It also works  $\forall n_q > 2$  !

### 3.1.3 in 2D/3D - theory

Let us now turn to a two-dimensional integral of the form

$$I = \int_{-1}^{+1} \int_{-1}^{+1} f(x, y) dx dy$$

The equivalent Gaussian quadrature writes:

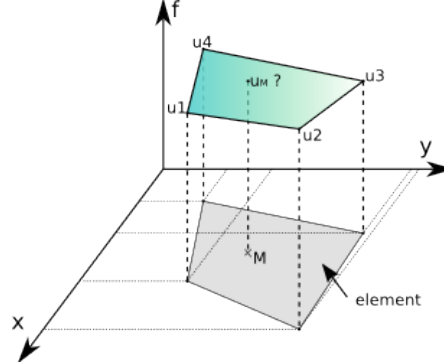
$$I_{gq} \simeq \sum_{i_q=1}^{n_q} \sum_{j_q=1}^{n_q} f(x_{i_q}, y_{j_q}) w_{i_q} w_{j_q}$$

### 3.2 The mesh

### 3.3 Elements and basis functions in 1D

### 3.4 Elements and basis functions in 2D

Let us for a moment consider a single quadrilateral element in the  $xy$ -plane, as shown on the following figure:



Let us assume that we know the values of a given field  $u$  at the vertices. For a given point  $M$  inside the element in the plane, what is the value of the field  $u$  at this point? It makes sense to postulate that  $u_M = u(x_M, y_M)$  will be given by

$$u_M = \phi(u_1, u_2, u_3, u_4, x_M, y_M)$$

where  $\phi$  is a function to be determined. Although  $\phi$  is not unique, we can decide to express the value  $u_M$  as a weighed sum of the values at the vertices  $u_i$ . One option could be to assign all four vertices the same weight, say  $1/4$  so that  $u_M = (u_1 + u_2 + u_3 + u_4)/4$ , i.e.  $u_M$  is simply given by the arithmetic mean of the vertices values. This approach suffers from a major drawback as it does not use the location of point  $M$  inside the element. For instance, when  $(x_M, y_M) \rightarrow (x_2, y_2)$  we expect  $u_M \rightarrow u_2$ .

In light of this, we could now assume that the weights would depend on the position of  $M$  in a continuous fashion:

$$u(x_M, y_M) = \sum_{i=1}^4 N_i(x_M, y_M) u_i$$

where the  $N_i$  are continous ("well behaved") functions which have the property:

$$N_i(x_j, y_j) = \delta_{ij}$$

or, in other words:

$$N_3(x_1, y_1) = 0 \quad (18)$$

$$N_3(x_2, y_2) = 0 \quad (19)$$

$$N_3(x_3, y_3) = 1 \quad (20)$$

$$N_3(x_4, y_4) = 0 \quad (21)$$

The functions  $N_i$  are commonly called basis functions.

Omitting the  $M$  subscripts for any point inside the element, the velocity components  $u$  and  $v$  are given by:

$$\hat{u}(x, y) = \sum_{i=1}^4 N_i(x, y) u_i \quad (22)$$

$$\hat{v}(x, y) = \sum_{i=1}^4 N_i(x, y) v_i \quad (23)$$

Rather interestingly, one can now easily compute velocity gradients (and therefore the strain rate tensor) since we have assumed the basis functions to be "well behaved" (in this case differentiable):

$$\dot{\epsilon}_{xx}(x, y) = \frac{\partial u}{\partial x} = \sum_{i=1}^4 \frac{\partial N_i}{\partial x} u_i \quad (24)$$

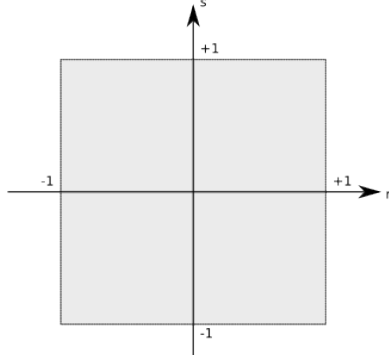
$$\dot{\epsilon}_{yy}(x, y) = \frac{\partial v}{\partial y} = \sum_{i=1}^4 \frac{\partial N_i}{\partial y} v_i \quad (25)$$

$$\dot{\epsilon}_{xy}(x, y) = \frac{1}{2} \frac{\partial u}{\partial y} + \frac{1}{2} \frac{\partial v}{\partial x} = \frac{1}{2} \sum_{i=1}^4 \frac{\partial N_i}{\partial y} u_i + \frac{1}{2} \sum_{i=1}^4 \frac{\partial N_i}{\partial x} v_i \quad (26)$$

How we actually obtain the exact form of the basis functions is explained in the coming section.

### 3.4.1 The $Q_1$ basis in 2D

In this section, we place ourselves in the most favorable case, i.e. the element is a square defined by  $-1 < r < 1$ ,  $-1 < s < 1$  in the Cartesian coordinates system  $(r, s)$ :



add corner numbering

This element is commonly called the reference element. How we go from the  $(x, y)$  coordinate system to the  $(r, s)$  once and vice versa will be dealt later on. For now, the basis functions in the above reference element and in the reduced coordinates system  $(r, s)$  are given by:

$$\begin{aligned} N_1(r, s) &= 0.25(1-r)(1-s) \\ N_2(r, s) &= 0.25(1+r)(1-s) \\ N_3(r, s) &= 0.25(1+r)(1+s) \\ N_4(r, s) &= 0.25(1-r)(1+s) \end{aligned}$$

The partial derivatives of these functions with respect to  $r$  and  $s$  automatically follow:

$$\begin{aligned} \frac{\partial N_1}{\partial r}(r, s) &= -0.25(1-s) \\ \frac{\partial N_2}{\partial r}(r, s) &= +0.25(1-s) \\ \frac{\partial N_3}{\partial r}(r, s) &= +0.25(1+s) \\ \frac{\partial N_4}{\partial r}(r, s) &= -0.25(1+s) \end{aligned}$$

$$\begin{aligned} \frac{\partial N_1}{\partial s}(r, s) &= -0.25(1-r) \\ \frac{\partial N_2}{\partial s}(r, s) &= -0.25(1+r) \\ \frac{\partial N_3}{\partial s}(r, s) &= +0.25(1+r) \\ \frac{\partial N_4}{\partial s}(r, s) &= +0.25(1-r) \end{aligned}$$

Let us go back to Eq.(23). And let us assume that the function  $v(r, s) = C$  so that  $v_i = C$  for  $i = 1, 2, 3, 4$ . It then follows that

$$\hat{v}(r, s) = \sum_{i=1}^4 N_i(r, s) v_i = C \sum_{i=1}^4 N_i(r, s) = C[N_1(r, s) + N_2(r, s) + N_3(r, s) + N_4(r, s)] = C$$

This is a very important property: if the  $v$  function used to assign values at the vertices is constant, then the value of  $\hat{v}$  anywhere in the element is exactly  $C$ . If we now turn to the derivatives of  $v$  with respect to  $r$  and  $s$ :

$$\frac{\partial \hat{v}}{\partial r}(r, s) = \sum_{i=1}^4 \frac{\partial N_i}{\partial r}(r, s) v_i = C \sum_{i=1}^4 \frac{\partial N_i}{\partial r}(r, s) = C[-0.25(1-s) + 0.25(1-s) + 0.25(1+s) - 0.25(1+s)] = 0$$

$$\frac{\partial \hat{v}}{\partial s}(r, s) = \sum_{i=1}^4 \frac{\partial N_i}{\partial s}(r, s) v_i = C \sum_{i=1}^4 \frac{\partial N_i}{\partial s}(r, s) = C [-0.25(1-r) - 0.25(1+r) + 0.25(1+r) + 0.25(1-r)] = 0$$

We reassuringly find that the derivative of a constant field anywhere in the element is exactly zero.

If we now choose  $v(r, s) = ar + bs$  with  $a$  and  $b$  two constant scalars, we find:

$$\hat{v}(r, s) = \sum_{i=1}^4 N_i(r, s) v_i \quad (27)$$

$$= \sum_{i=1}^4 N_i(r, s)(ar_i + bs_i) \quad (28)$$

$$= a \underbrace{\sum_{i=1}^4 N_i(r, s)r_i}_{r} + b \underbrace{\sum_{i=1}^4 N_i(r, s)s_i}_{s} \quad (29)$$

$$\begin{aligned} &= a [0.25(1-r)(1-s)(-1) + 0.25(1+r)(1-s)(+1) + 0.25(1+r)(1+s)(+1) + 0.25(1-r)(1+s)(-1)] \\ &+ b [0.25(1-r)(1-s)(-1) + 0.25(1+r)(1-s)(-1) + 0.25(1+r)(1+s)(+1) + 0.25(1-r)(1+s)(+1)] \\ &= a [-0.25(1-r)(1-s) + 0.25(1+r)(1-s) + 0.25(1+r)(1+s) - 0.25(1-r)(1+s)] \\ &+ b [-0.25(1-r)(1-s) - 0.25(1+r)(1-s) + 0.25(1+r)(1+s) + 0.25(1-r)(1+s)] \\ &= ar + bs \end{aligned} \quad (30)$$

**verify above eq.** This set of bilinear shape functions is therefore capable of exactly representing a bilinear field. The derivatives are:

$$\frac{\partial \hat{v}}{\partial r}(r, s) = \sum_{i=1}^4 \frac{\partial N_i}{\partial r}(r, s) v_i \quad (31)$$

$$= a \sum_{i=1}^4 \frac{\partial N_i}{\partial r}(r, s)r_i + b \sum_{i=1}^4 \frac{\partial N_i}{\partial r}(r, s)s_i \quad (32)$$

$$\begin{aligned} &= a [-0.25(1-s)(-1) + 0.25(1-s)(+1) + 0.25(1+s)(+1) - 0.25(1+s)(-1)] \\ &+ b [-0.25(1-s)(-1) + 0.25(1-s)(-1) + 0.25(1+s)(+1) - 0.25(1+s)(+1)] \\ &= \frac{a}{4} [(1-s) + (1-s) + (1+s) + (1+s)] \\ &+ \frac{b}{4} [(1-s) - (1-s) + (1+s) - (1+s)] \\ &= a \end{aligned} \quad (33)$$

Here again, we find that the derivative of the bilinear field inside the element is exact:  $\frac{\partial \hat{v}}{\partial r} = \frac{\partial v}{\partial r}$ .

However, following the same methodology as above, one can easily prove that this is no more true for polynomials of degree strivtly higher than 1. This fact has serious consequences: if the solution to the problem at hand is for instance a parabola, the  $Q_1$  shape functions cannot represent the solution properly, but only by approximating the parabola in each element by a line. As we will see later,  $Q_2$  basis functions can remedy this problem by containing themselves quadratic terms.

### 3.4.2 The $Q_2$ basis in 2D

## 3.5 The penalty approach

In order to impose the incompressibility constraint, two widely used procedures are available, namely the Lagrange multiplier method and the penalty method [2, 25]. The latter is implemented in ELEFANT, which allows for the elimination of the pressure variable from the momentum equation (resulting in a reduction of the matrix size).

Mathematical details on the origin and validity of the penalty approach applied to the Stokes problem can for instance be found in [10], [43] or [23].

The penalty formulation of the mass conservation equation is based on a relaxation of the incompressibility constraint and writes

$$\nabla \cdot \mathbf{v} + \frac{p}{\lambda} = 0 \quad (34)$$

where  $\lambda$  is the penalty parameter, that can be interpreted (and has the same dimension) as a bulk viscosity. It is equivalent to say that the material is weakly compressible. It can be shown that if one chooses  $\lambda$  to be a sufficiently

large number, the continuity equation  $\nabla \cdot \mathbf{v} = 0$  will be approximately satisfied in the finite element solution. The value of  $\lambda$  is often recommended to be 6 to 7 orders of magnitude larger than the shear viscosity [17, 26].

Equation (34) can be used to eliminate the pressure in Eq. (??) so that the mass and momentum conservation equations fuse to become :

$$\nabla \cdot (2\eta \dot{\varepsilon}(\mathbf{v})) + \lambda \nabla (\nabla \cdot \mathbf{v}) = \rho \mathbf{g} = 0 \quad (35)$$

[36] have established the equivalence for incompressible problems between the reduced integration of the penalty term and a mixed Finite Element approach if the pressure nodes coincide with the integration points of the reduced rule.

In the end, the elimination of the pressure unknown in the Stokes equations replaces the original saddle-point Stokes problem [3] by an elliptical problem, which leads to a symmetric positive definite (SPD) FEM matrix. This is the major benefit of the penalized approach over the full indefinite solver with the velocity-pressure variables. Indeed, the SPD character of the matrix lends itself to efficient solving strategies and is less memory-demanding since it is sufficient to store only the upper half of the matrix including the diagonal [22]. ToDo: list codes which use this approach.

The stress tensor  $\boldsymbol{\sigma}$  is symmetric (*i.e.*  $\sigma_{ij} = \sigma_{ji}$ ). For simplicity I will now focus on a Stokes flow in two dimensions.

Since the penalty formulation is only valid for incompressible flows, then  $\dot{\epsilon} = \dot{\epsilon}^d$  so that the  $d$  superscript is omitted in what follows. The stress tensor can also be cast in vector format:

$$\begin{aligned} \begin{pmatrix} \sigma_{xx} \\ \sigma_{yy} \\ \sigma_{xy} \end{pmatrix} &= \begin{pmatrix} -p \\ -p \\ 0 \end{pmatrix} + 2\eta \begin{pmatrix} \dot{\epsilon}_{xx} \\ \dot{\epsilon}_{yy} \\ \dot{\epsilon}_{xy} \end{pmatrix} \\ &= \lambda \begin{pmatrix} \dot{\epsilon}_{xx} + \dot{\epsilon}_{yy} \\ \dot{\epsilon}_{xx} + \dot{\epsilon}_{yy} \\ 0 \end{pmatrix} + 2\eta \begin{pmatrix} \dot{\epsilon}_{xx} \\ \dot{\epsilon}_{yy} \\ \dot{\epsilon}_{xy} \end{pmatrix} \\ &= \left[ \underbrace{\lambda \begin{pmatrix} 1 & 1 & 0 \\ 1 & 1 & 0 \\ 0 & 0 & 0 \end{pmatrix}}_{\mathbf{K}} + \underbrace{\eta \begin{pmatrix} 2 & 0 & 0 \\ 0 & 2 & 0 \\ 0 & 0 & 1 \end{pmatrix}}_{\mathbf{C}} \right] \cdot \begin{pmatrix} \frac{\partial u}{\partial x} \\ \frac{\partial v}{\partial y} \\ \frac{\partial u}{\partial y} + \frac{\partial v}{\partial x} \end{pmatrix} \end{aligned}$$

Remember that

$$\frac{\partial u}{\partial x} = \sum_{i=1}^4 \frac{\partial N_i}{\partial x} u_i \quad \frac{\partial v}{\partial y} = \sum_{i=1}^4 \frac{\partial N_i}{\partial y} v_i$$

$$\frac{\partial u}{\partial y} + \frac{\partial v}{\partial x} = \sum_{i=1}^4 \frac{\partial N_i}{\partial y} u_i + \sum_{i=1}^4 \frac{\partial N_i}{\partial x} v_i$$

so that

$$\begin{pmatrix} \frac{\partial u}{\partial x} \\ \frac{\partial v}{\partial y} \\ \frac{\partial u}{\partial y} + \frac{\partial v}{\partial x} \end{pmatrix} = \underbrace{\begin{pmatrix} \frac{\partial N_1}{\partial x} & 0 & \frac{\partial N_2}{\partial x} & 0 & \frac{\partial N_3}{\partial x} & 0 & \frac{\partial N_4}{\partial x} & 0 \\ 0 & \frac{\partial N_1}{\partial y} & 0 & \frac{\partial N_2}{\partial y} & 0 & \frac{\partial N_3}{\partial y} & 0 & \frac{\partial N_4}{\partial y} \\ \frac{\partial N_1}{\partial y} & \frac{\partial N_1}{\partial x} & \frac{\partial N_2}{\partial y} & \frac{\partial N_2}{\partial x} & \frac{\partial N_3}{\partial y} & \frac{\partial N_3}{\partial x} & \frac{\partial N_3}{\partial y} & \frac{\partial N_4}{\partial x} \end{pmatrix}}_{\mathbf{B}} \cdot \underbrace{\begin{pmatrix} u1 \\ v1 \\ u2 \\ v2 \\ u3 \\ v3 \\ u4 \\ v4 \end{pmatrix}}_{\mathbf{V}}$$

Finally,

$$\vec{\sigma} = \begin{pmatrix} \sigma_{xx} \\ \sigma_{yy} \\ \sigma_{xy} \end{pmatrix} = (\lambda \mathbf{K} + \eta \mathbf{C}) \cdot \mathbf{B} \cdot \mathbf{V}$$

We will now establish the weak form of the momentum conservation equation. We start again from

$$\nabla \cdot \boldsymbol{\sigma} + \mathbf{b} = \mathbf{0}$$

For the  $N_i$ 's 'regular enough', we can write:

$$\int_{\Omega_e} N_i \nabla \cdot \boldsymbol{\sigma} d\Omega + \int_{\Omega_e} N_i \mathbf{b} d\Omega = 0$$

We can integrate by parts and drop the surface term<sup>1</sup>:

$$\int_{\Omega_e} \nabla N_i \cdot \boldsymbol{\sigma} d\Omega = \int_{\Omega_e} N_i \mathbf{b} d\Omega$$

or,

$$\int_{\Omega_e} \begin{pmatrix} \frac{\partial N_i}{\partial x} & 0 & \frac{\partial N_i}{\partial y} \\ 0 & \frac{\partial N_i}{\partial y} & \frac{\partial N_i}{\partial x} \end{pmatrix} \cdot \begin{pmatrix} \sigma_{xx} \\ \sigma_{yy} \\ \sigma_{xy} \end{pmatrix} d\Omega = \int_{\Omega_e} N_i \mathbf{b} d\Omega$$

---

<sup>1</sup>We will come back to this at a later stage

Let  $i = 1, 2, 3, 4$  and stack the resulting four equations on top of one another.

$$\int_{\Omega_e} \begin{pmatrix} \frac{\partial N_1}{\partial x} & 0 & \frac{\partial N_1}{\partial y} \\ 0 & \frac{\partial N_1}{\partial y} & \frac{\partial N_1}{\partial x} \end{pmatrix} \cdot \begin{pmatrix} \sigma_{xx} \\ \sigma_{yy} \\ \sigma_{xy} \end{pmatrix} d\Omega = \int_{\Omega_e} N_1 \begin{pmatrix} b_x \\ b_y \end{pmatrix} d\Omega \quad (36)$$

$$\int_{\Omega_e} \begin{pmatrix} \frac{\partial N_2}{\partial x} & 0 & \frac{\partial N_2}{\partial y} \\ 0 & \frac{\partial N_2}{\partial y} & \frac{\partial N_2}{\partial x} \end{pmatrix} \cdot \begin{pmatrix} \sigma_{xx} \\ \sigma_{yy} \\ \sigma_{xy} \end{pmatrix} d\Omega = \int_{\Omega_e} N_2 \begin{pmatrix} b_x \\ b_y \end{pmatrix} d\Omega \quad (37)$$

$$\int_{\Omega_e} \begin{pmatrix} \frac{\partial N_3}{\partial x} & 0 & \frac{\partial N_3}{\partial y} \\ 0 & \frac{\partial N_3}{\partial y} & \frac{\partial N_3}{\partial x} \end{pmatrix} \cdot \begin{pmatrix} \sigma_{xx} \\ \sigma_{yy} \\ \sigma_{xy} \end{pmatrix} d\Omega = \int_{\Omega_e} N_3 \begin{pmatrix} b_x \\ b_y \end{pmatrix} d\Omega \quad (38)$$

$$\int_{\Omega_e} \begin{pmatrix} \frac{\partial N_4}{\partial x} & 0 & \frac{\partial N_4}{\partial y} \\ 0 & \frac{\partial N_4}{\partial y} & \frac{\partial N_4}{\partial x} \end{pmatrix} \cdot \begin{pmatrix} \sigma_{xx} \\ \sigma_{yy} \\ \sigma_{xy} \end{pmatrix} d\Omega = \int_{\Omega_e} N_4 \begin{pmatrix} b_x \\ b_y \end{pmatrix} d\Omega \quad (39)$$

We easily recognize  $\mathbf{B}^T$  inside the integrals! Let us define

$$\mathbf{N}_b^T = (N_1 b_x, N_1 b_y, \dots, N_4 b_x, N_4 b_y)$$

then we can write

$$\int_{\Omega_e} \mathbf{B}^T \cdot \begin{pmatrix} \sigma_{xx} \\ \sigma_{yy} \\ \sigma_{xy} \end{pmatrix} d\Omega = \int_{\Omega_e} \mathbf{N}_b d\Omega$$

and finally:

$$\int_{\Omega_e} \mathbf{B}^T \cdot [\lambda \mathbf{K} + \eta \mathbf{C}] \cdot \mathbf{B} \cdot \mathbf{V} d\Omega = \int_{\Omega_e} \mathbf{N}_b d\Omega$$

Since  $\mathbf{V}$  contains the velocities at the corners, it does not depend on the  $x$  or  $y$  coordinates so it can be taking outside of the integral:

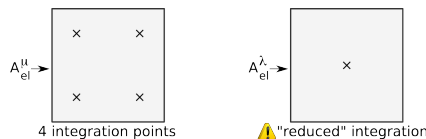
$$\underbrace{\left( \int_{\Omega_e} \mathbf{B}^T \cdot [\lambda \mathbf{K} + \eta \mathbf{C}] \cdot \mathbf{B} d\Omega \right)}_{A_{el}(8 \times 8)} \cdot \underbrace{\mathbf{V}}_{(8 \times 1)} = \underbrace{\int_{\Omega_e} \mathbf{N}_b d\Omega}_{B_{el}(8 \times 1)}$$

or,

$$\left[ \underbrace{\left( \int_{\Omega_e} \lambda \mathbf{B}^T \cdot \mathbf{K} \cdot \mathbf{B} d\Omega \right)}_{A_{el}^\lambda(8 \times 8)} + \underbrace{\left( \int_{\Omega_e} \eta \mathbf{B}^T \cdot \mathbf{C} \cdot \mathbf{B} d\Omega \right)}_{A_{el}^\eta(8 \times 8)} \right] \cdot \underbrace{\mathbf{V}}_{(8 \times 1)} = \underbrace{\int_{\Omega_e} \mathbf{N}_b d\Omega}_{B_{el}(8 \times 1)}$$

## INTEGRATION - MAPPING

1. partition domain  $\Omega$  into elements  $\Omega_e, e = 1, \dots, n_{el}$ .
2. loop over elements and for each element compute  $\mathbf{A}_{el}, \mathbf{B}_{el}$



3. a node belongs to several elements  
→ need to assemble  $\mathbf{A}_{el}$  and  $\mathbf{B}_{el}$  in  $\mathbf{A}, \mathbf{B}$
4. apply boundary conditions
5. solve system:  $\mathbf{x} = \mathbf{A}^{-1} \cdot \mathbf{B}$
6. visualise/analyse  $\mathbf{x}$

## **4 Additional techniques**

- 4.1 The method of manufactured solutions**
- 4.2 Sparse storage**
- 4.3 Mesh generation**
- 4.4 The value of the timestep**
- 4.5 Tracking materials**
- 4.6 Visco-Plasticity**
- 4.7 Picard and Newton**
- 4.8 The choice of solvers**
- 4.9 The SUPG formulation for the energy equation**
- 4.10 Tracking materials and/or interfaces**
- 4.11 Dealing with a free surface**
- 4.12 Pressure normalisation**

so much to do ...  
write about impose bc on el matrix  
Q3Q2  
full compressible  
total energy calculations  
constraints  
compositions, marker chain  
van keken initial value with deformed mesh  
free-slip bc on annulus and sphere . See for example p540 Gresho and Sani book.  
non-linear rheologies (two layer brick spmw16, tosn15)  
Picard vs Newton  
markers  
Schur complement approach  
periodic boundary conditions  
open boundary conditions  
free surface  
SUPG  
produce fastest version possible for convection box  
zaleski disk advection  
all kinds of interesting benchmarks  
Busse convection pb, compare with aspect  
cvi !!!  
pure elastic  
including phase changes (w. R. Myhill)  
derivatives on nodes  
Nusselt  
discontinuous galerkin  
formatting of code style  
navier-stokes ? (LUKAS)  
pressure smoothing  
compute strainrate in middle of element or at quad point for punch?  
GEO1442 code  
GEO1442 indenter setup in plane ?  
in/out flow on sides for lith modelling  
Problems to solve:  
colorscale  
better yet simple matrix storage ?

## 5 fieldstone: simple analytical solution

From [15]. In order to illustrate the behavior of selected mixed finite elements in the solution of stationary Stokes flow, we consider a two-dimensional problem in the square domain  $\Omega = [0, 1] \times [0, 1]$ , which possesses a closed-form analytical solution. The problem consists of determining the velocity field  $\mathbf{v} = (u, v)$  and the pressure  $p$  such that

$$-\nu \Delta \mathbf{v} + \nabla p = \mathbf{b} \quad \text{in } \Omega$$

$$\nabla \cdot \mathbf{v} = 0 \quad \text{in } \Omega$$

$$\mathbf{v} = \mathbf{0} \quad \text{on } \Gamma$$

where the fluid viscosity is taken as  $\nu = 1$ . The components of the body force  $\mathbf{b}$  are prescribed as

$$\begin{aligned} b_x &= (12 - 24y)x^4 + (-24 + 48y)x^3 + (-48y + 72y^2 - 48y^3 + 12)x^2 \\ &\quad + (-2 + 24y - 72y^2 + 48y^3)x + 1 - 4y + 12y^2 - 8y^3 \\ b_y &= (8 - 48y + 48y^2)x^3 + (-12 + 72y - 72y^2)x^2 \\ &\quad + (4 - 24y + 48y^2 - 48y^3 + 24y^4)x - 12y^2 + 24y^3 - 12y^4 \end{aligned}$$

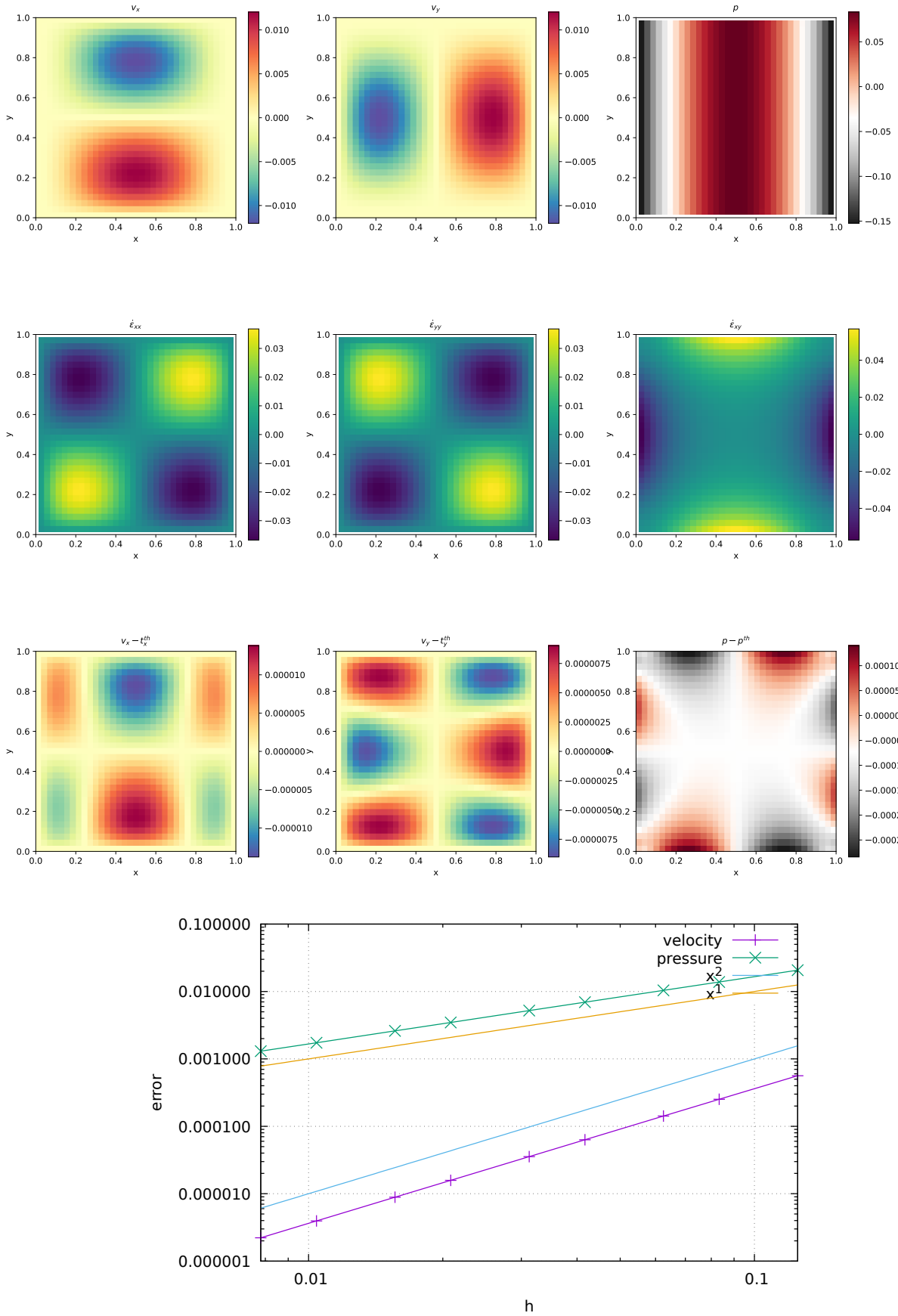
With this prescribed body force, the exact solution is

$$\begin{aligned} u(x, y) &= x^2(1-x)^2(2y-6y^2+4y^3) \\ v(x, y) &= -y^2(1-y)^2(2x-6x^2+4x^3) \\ p(x, y) &= x(1-x) - 1/6 \end{aligned}$$

Note that the pressure obeys  $\int_{\Omega} p \, d\Omega = 0$

### features

- $Q_1 \times P_0$  element
- incompressible flow
- penalty formulation
- Dirichlet boundary conditions (no-slip)
- direct solver
- isothermal
- isoviscous
- analytical solution



Quadratic convergence for velocity error, linear convergence for pressure error, as expected.

ToDo:

pressure normalisation?

different cmat, a la schmalholz

To go further:

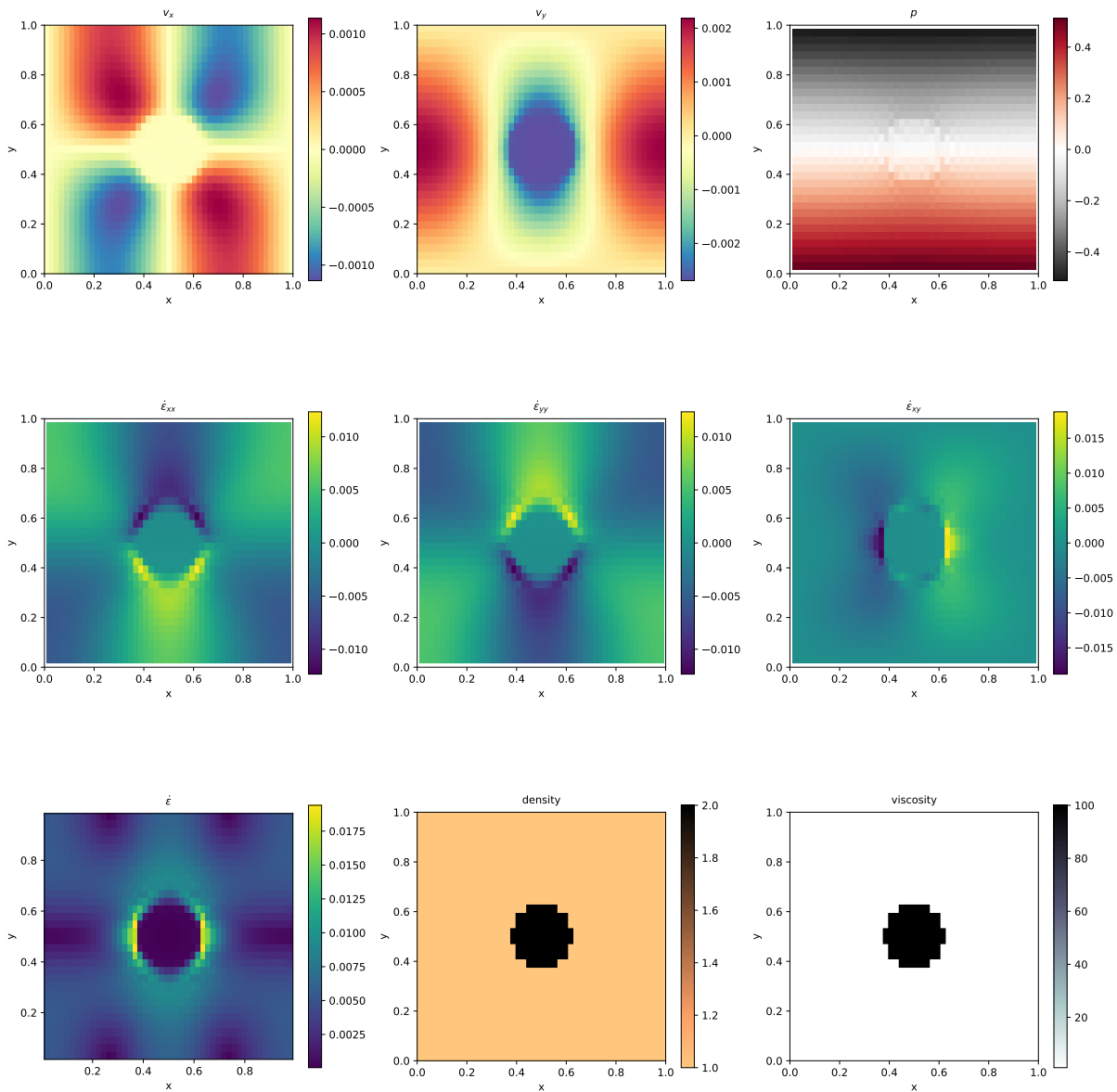
1. make your own analytical solution

## 6 fieldstone: Stokes sphere

Viscosity and density directly computed at the quadrature points.

### features

- $Q_1 \times P_0$  element
- incompressible flow
- penalty formulation
- Dirichlet boundary conditions (free-slip)
- direct solver
- isothermal
- non-isoviscous
- buoyancy-driven flow



## 7 fieldstone: Convection in a 2D box

This benchmark deals with the 2-D thermal convection of a fluid of infinite Prandtl number in a rectangular closed cell. In what follows, I carry out the case 1a, 1b, and 1c experiments as shown in [5]: steady convection with constant viscosity in a square box.

The temperature is fixed to zero on top and to  $\Delta T$  at the bottom, with reflecting symmetry at the sidewalls (i.e.  $\partial_x T = 0$ ) and there are no internal heat sources. Free-slip conditions are implemented on all boundaries.

The Rayleigh number is given by

$$Ra = \frac{\alpha g_y \Delta T h^3}{\kappa \nu} = \frac{\alpha g_y \Delta T h^3 \rho^2 c_p}{k \mu} \quad (40)$$

In what follows, I use the following parameter values:  $L_x = L_y = 1, \rho_0 = c_p = k = \mu = 1, T_0 = 0, \alpha = 10^{-2}, g = 10^2 Ra$  and I run the model with  $Ra = 10^4, 10^5$  and  $10^6$ .

The initial temperature field is given by

$$T(x, y) = (1 - y) - 0.01 \cos(\pi x) \sin(\pi y) \quad (41)$$

The perturbation in the initial temperature fields leads to a perturbation of the density field and sets the fluid in motion.

Depending on the initial Rayleigh number, the system ultimately reaches a steady state after some time.

The Nusselt number (i.e. the mean surface temperature gradient over mean bottom temperature) is computed as follows [5]:

$$Nu = L_y \frac{\int \frac{\partial T}{\partial y} (y = L_y) dx}{\int T(y = 0) dx} \quad (42)$$

Note that in our case the denominator is equal to 1 since  $L_x = 1$  and the temperature at the bottom is prescribed to be 1.

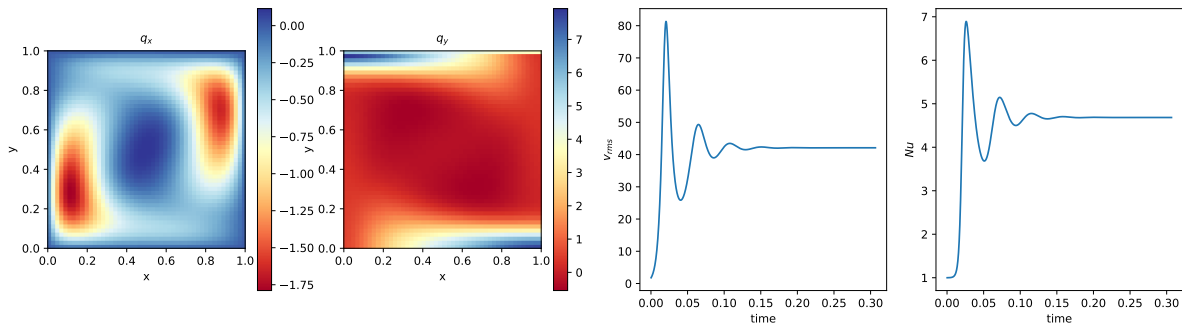
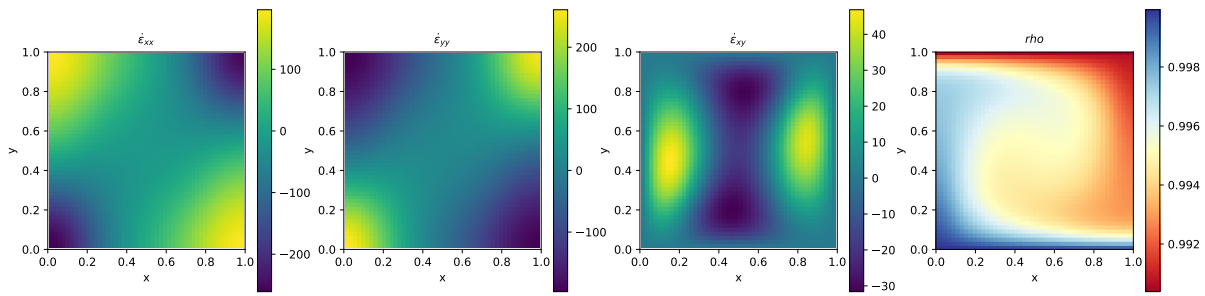
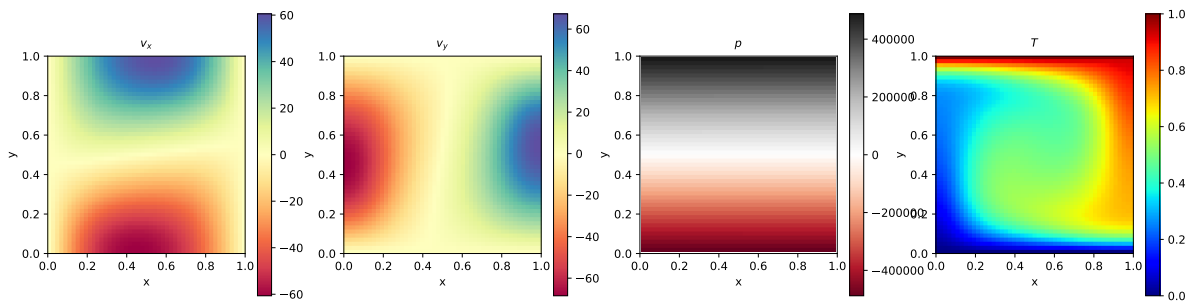
Finally, the steady state root mean square velocity and Nusselt number measurements are indicated in Table ?? alongside those of [5] and [49]. (Note that this benchmark was also carried out and published in other publications [54, 1, 20, 11, 34] but since they did not provide a complete set of measurement values, they are not included in the table.)

		Blankenbach et al	Tackley [49]
$Ra = 10^4$	$V_{rms}$	$42.864947 \pm 0.000020$	42.775
	$Nu$	$4.884409 \pm 0.000010$	4.878
$Ra = 10^5$	$V_{rms}$	$193.21454 \pm 0.00010$	193.11
	$Nu$	$10.534095 \pm 0.000010$	10.531
$Ra = 10^6$	$V_{rms}$	$833.98977 \pm 0.00020$	833.55
	$Nu$	$21.972465 \pm 0.000020$	21.998

Steady state Nusselt number  $Nu$  and  $V_{rms}$  measurements as reported in the literature.

### features

- $Q_1 \times P_0$  element
- incompressible flow
- penalty formulation
- Dirichlet boundary conditions (free-slip)
- Boussinesq approximation
- direct solver
- non-isothermal
- buoyancy-driven flow
- isoviscous
- CFL-condition



ToDo:

implement steady state criterion

reach steady state

do Ra=1e4, 1e5, 1e6

plot against blankenbach paper and aspect

look at critical Ra number

## 8 fieldstone: solcx benchmark

The SolCx benchmark is intended to test the accuracy of the solution to a problem that has a large jump in the viscosity along a line through the domain. Such situations are common in geophysics: for example, the viscosity in a cold, subducting slab is much larger than in the surrounding, relatively hot mantle material.

The SolCx benchmark computes the Stokes flow field of a fluid driven by spatial density variations, subject to a spatially variable viscosity. Specifically, the domain is  $\Omega = [0, 1]^2$ , gravity is  $\mathbf{g} = (0, -1)^T$  and the density is given by

$$\rho(x, y) = \sin(\pi y) \cos(\pi x) \quad (43)$$

Boundary conditions are free slip on all of the sides of the domain and the temperature plays no role in this benchmark. The viscosity is prescribed as follows:

$$\mu(x, y) = \begin{cases} 1 & \text{for } x < 0.5 \\ 10^6 & \text{for } x > 0.5 \end{cases} \quad (44)$$

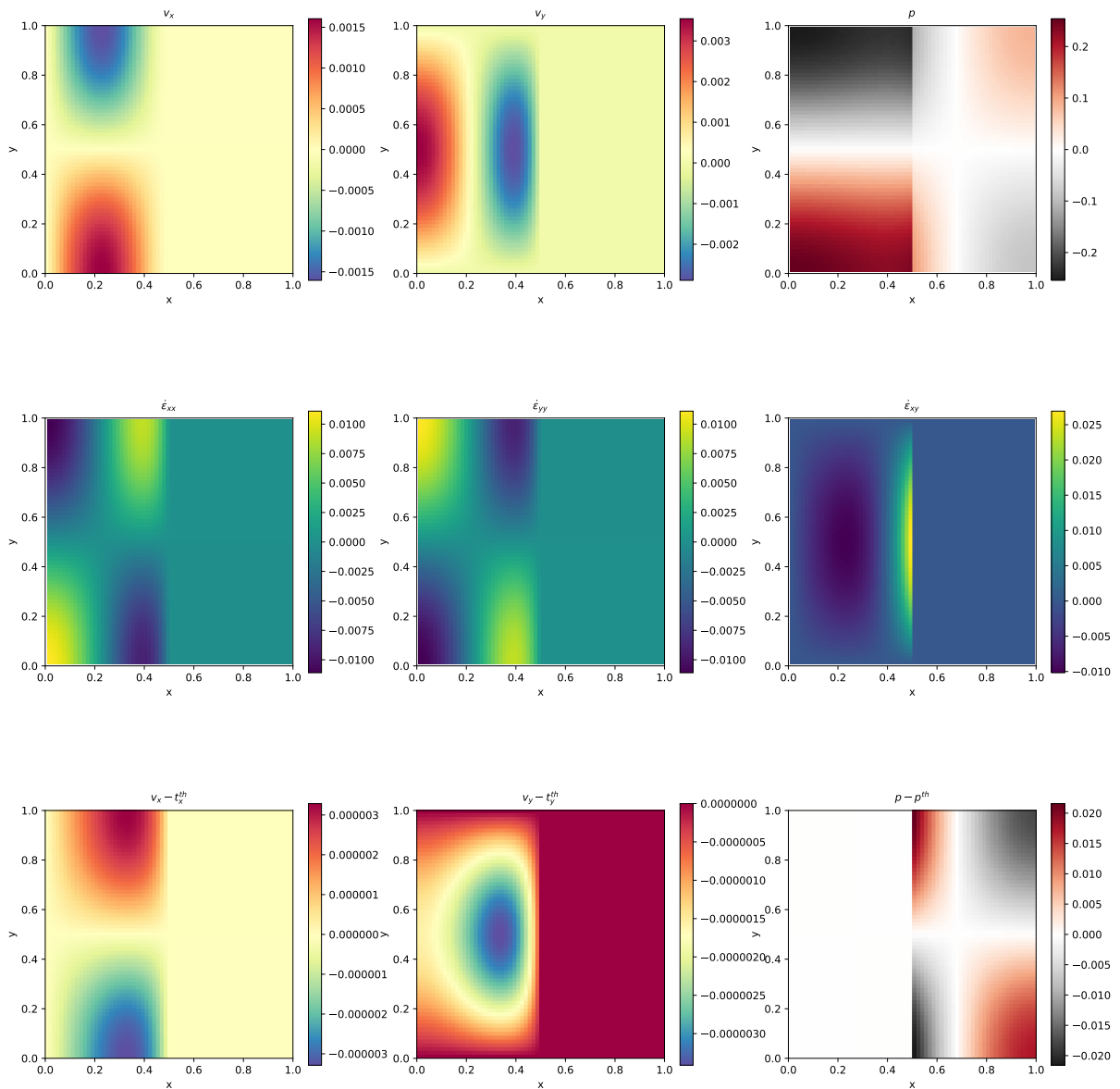
Note the strongly discontinuous viscosity field yields a stagnant flow in the right half of the domain and thereby yields a pressure discontinuity along the interface.

The SolCx benchmark was previously used in [18] (references to earlier uses of the benchmark are available there) and its analytic solution is given in [57]. It has been carried out in [32] and [21]. Note that the source code which evaluates the velocity and pressure fields for both SolCx and SolKz is distributed as part of the open source package Underworld ([39], <http://underworldproject.org>).

In this particular example, the viscosity is computed analytically at the quadrature points (i.e. tracers are not used to attribute a viscosity to the element). If the number of elements is even in any direction, all elements (and their associated quadrature points) have a constant viscosity(1 or  $10^6$ ). If it is odd, then the elements situated at the viscosity jump have half their integration points with  $\mu = 1$  and half with  $\mu = 10^6$  (which is a pathological case since the used quadrature rule inside elements cannot represent accurately such a jump).

### features

- $Q_1 \times P_0$  element
- incompressible flow
- penalty formulation
- Dirichlet boundary conditions (free-slip)
- direct solver
- isothermal
- non-isoviscous
- analytical solution



What we learn from this

## 9 fieldstone: solkz benchmark

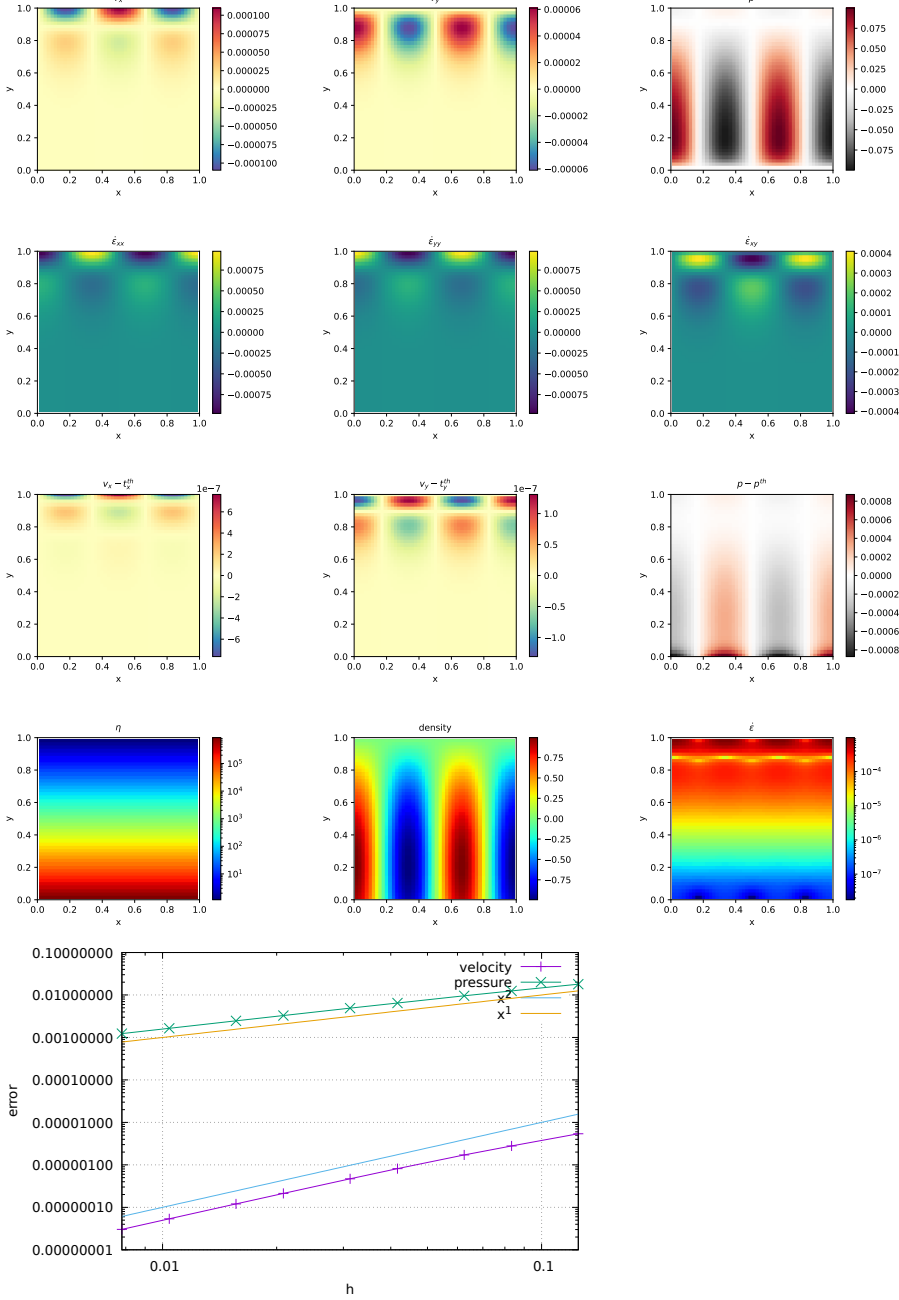
The SolKz benchmark [44] is similar to the SolCx benchmark, but the viscosity is now a function of the space coordinates:

$$\mu(y) = \exp(By) \quad \text{with} \quad B = 13.8155 \quad (45)$$

It is however not a discontinuous function but grows exponentially with the vertical coordinate so that its overall variation is again  $10^6$ . The forcing is again chosen by imposing a spatially variable density variation as follows:

$$\rho(x, y) = \sin(2y) \cos(3\pi x) \quad (46)$$

Free slip boundary conditions are imposed on all sides of the domain. This benchmark is presented in [57] as well and is studied in [18] and [21].



## 10 fieldstone: solvi benchmark

Following SolCx and SolKz, the SolVi inclusion benchmark solves a problem with a discontinuous viscosity field, but in this case the viscosity field is chosen in such a way that the discontinuity is along a circle. Given the regular nature of the grid used by a majority of codes and the present one, this ensures that the discontinuity in the viscosity never aligns to cell boundaries. This in turns leads to almost discontinuous pressures along the interface which are difficult to represent accurately. [46] derived a simple analytic solution for the pressure and velocity fields for a circular inclusion under simple shear and it was used in [13], [48], [18], [32] and [21].

Because of the symmetry of the problem, we only have to solve over the top right quarter of the domain (see Fig. ??a).

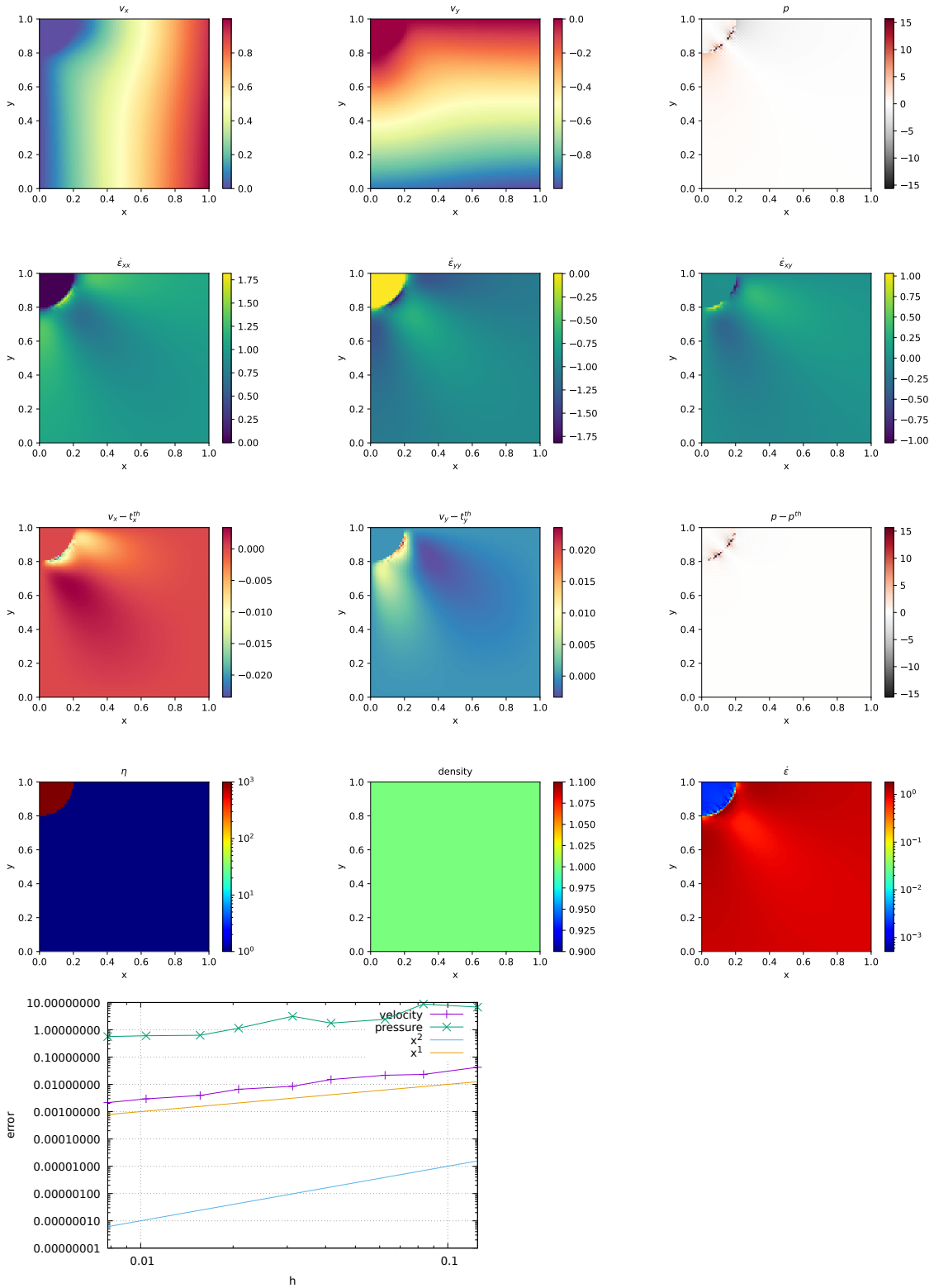
The analytical solution requires a strain rate boundary condition (e.g., pure shear) to be applied far away from the inclusion. In order to avoid using very large domains and/or dealing with this type of boundary condition altogether, the analytical solution is evaluated and imposed on the boundaries of the domain. By doing so, the truncation error introduced while discretizing the strain rate boundary condition is removed.

A characteristic of the analytic solution is that the pressure is zero inside the inclusion, while outside it follows the relation

$$p_m = 4\dot{\epsilon} \frac{\mu_m(\mu_i - \mu_m)}{\mu_i + \mu_m} \frac{r_i^2}{r^2} \cos(2\theta) \quad (47)$$

where  $\mu_i = 10^3$  is the viscosity of the inclusion and  $\mu_m = 1$  is the viscosity of the background media,  $\theta = \tan^{-1}(y/x)$ , and  $\dot{\epsilon} = 1$  is the applied strain rate.

[13] thoroughly investigated this problem with various numerical methods (FEM, FDM), with and without tracers, and conclusively showed how various averagings lead to different results. [18] obtained a first order convergence for both pressure and velocity, while [32] and [21] showed that the use of adaptive mesh refinement in respectively the FEM and FDM yields convergence rates which depend on refinement strategies.



## 11 fieldstone: the indentor benchmark

The punch benchmark is one of the few boundary value problems involving plastic solids for which there exists an exact solution. Such solutions are usually either for highly simplified geometries (spherical or axial symmetry, for instance) or simplified material models (such as rigid plastic solids) [30].

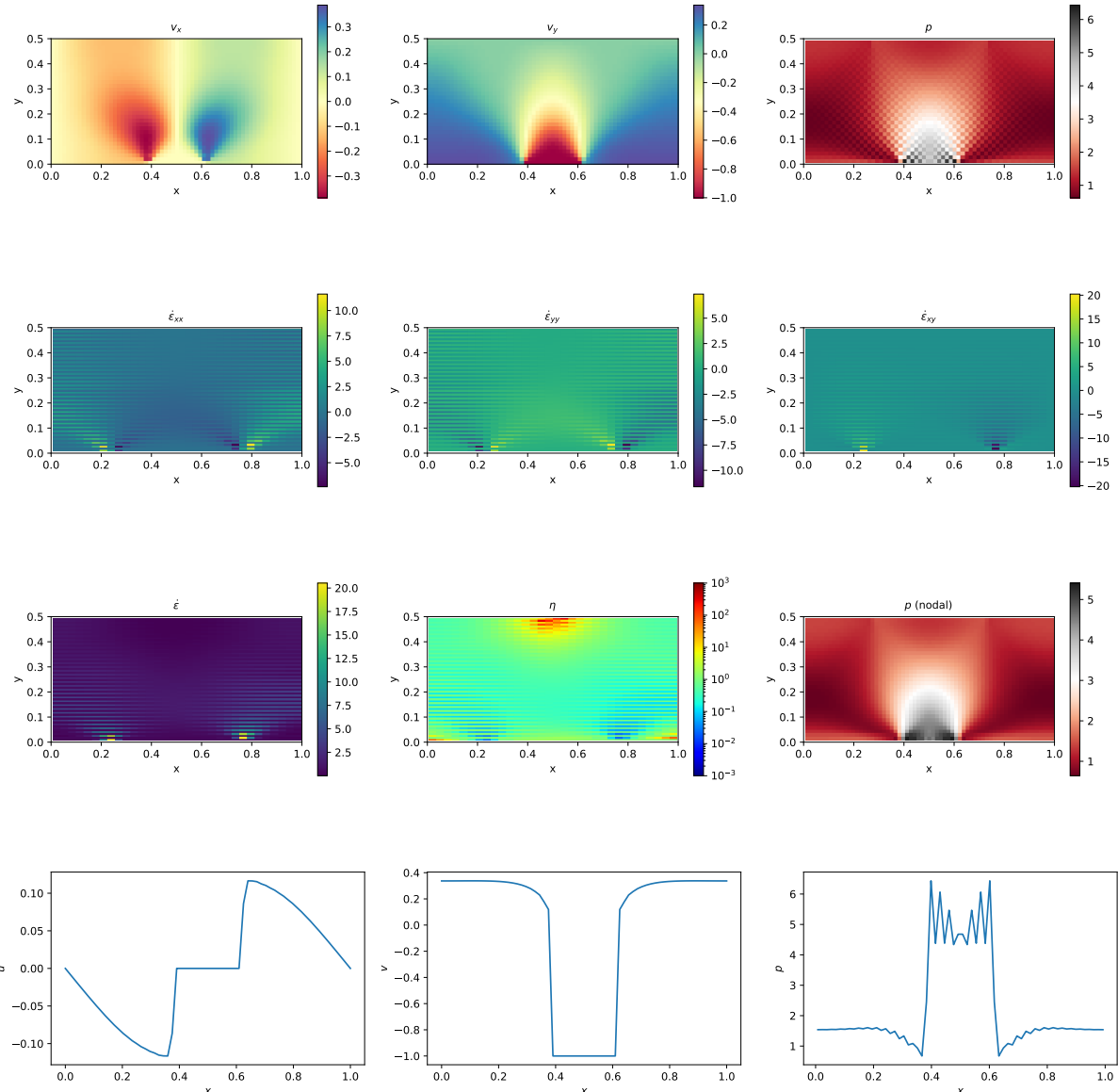
In this experiment, a rigid punch indents a rigid plastic half space; the slip line field theory gives exact solutions as shown in Fig. ??a. The plane strain formulation of the equations and the detailed solution to the problem were derived in the Appendix of [53] and are also presented in [19].

The two dimensional punch problem has been extensively studied numerically for the past 40 years [60, 59, 9, 8, 27, 56, 6, 42] and has been used to draw a parallel with the tectonics of eastern China in the context of the India-Eurasia collision [51, 38]. It is also worth noting that it has been carried out in one form or another in series of analogue modelling articles concerning the same region, with a rigid indenter colliding with a rheologically stratified lithosphere [40, 12, 29].

Numerically, the one-time step punch experiment is performed on a two-dimensional domain of purely plastic von Mises material. Given that the von Mises rheology yield criterion does not depend on pressure, the density of the material and/or the gravity vector is set to zero. Sides are set to free slip boundary conditions, the bottom to no slip, while a vertical velocity  $(0, -v_p)$  is prescribed at the top boundary for nodes whose  $x$  coordinate is within  $[L_x/2 - \delta/2, L_x/2 + \delta/2]$ .

The following parameters are used:  $L_x = 1$ ,  $L_y = 0.5$ ,  $\mu_{min} = 10^{-3}$ ,  $\mu_{max} = 10^3$ ,  $v_p = 1$ ,  $\delta = 0.123456789$  and the yield value of the material is set to  $k = 1$ .

The analytical solution predicts that the angle of the shear bands stemming from the sides of the punch is  $\pi/4$ , that the pressure right under the punch is  $1 + \pi$ , and that the velocity of the rigid blocks on each side of the punch is  $v_p/\sqrt{2}$  (this is simply explained by invoking conservation of mass).



ToDo: smooth punch

**features**

- $Q_1 \times P_0$  element
- incompressible flow
- penalty formulation
- Dirichlet boundary conditions (no-slip)
- isothermal
- non-isoviscous
- nonlinear rheology

## 12 fieldstone: the annulus benchmark

This benchmark is based on Thieulot & Puckett [Subm.] in which an analytical solution to the isoviscous incompressible Stokes equations is derived in an annulus geometry. The velocity and pressure fields are as follows:

$$v_r(r, \theta) = g(r)k \sin(k\theta), \quad (48)$$

$$v_\theta(r, \theta) = f(r) \cos(k\theta), \quad (49)$$

$$p(r, \theta) = kh(r) \sin(k\theta), \quad (50)$$

$$\rho(r, \theta) = \aleph(r)k \sin(k\theta), \quad (51)$$

with

$$f(r) = Ar + B/r, \quad (52)$$

$$g(r) = \frac{A}{2}r + \frac{B}{r} \ln r + \frac{C}{r}, \quad (53)$$

$$h(r) = \frac{2g(r) - f(r)}{r}, \quad (54)$$

$$\aleph(r) = g'' - \frac{g'}{r} - \frac{g}{r^2}(k^2 - 1) + \frac{f}{r^2} + \frac{f'}{r}, \quad (55)$$

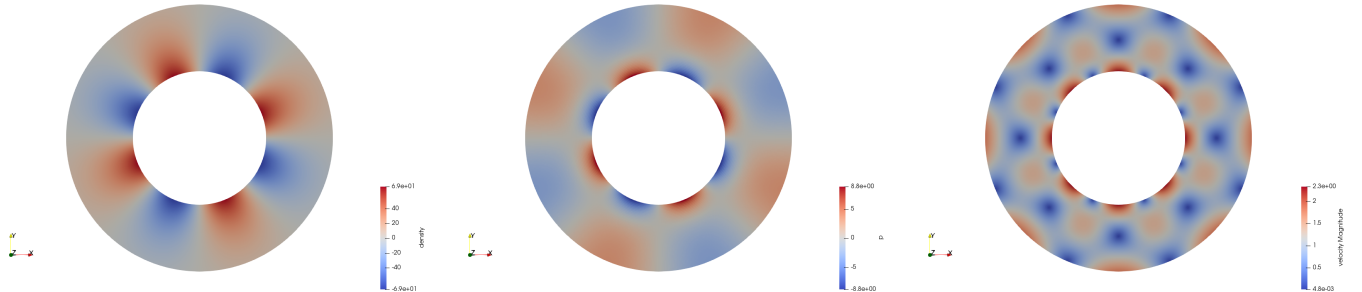
$$A = -C \frac{2(\ln R_1 - \ln R_2)}{R_2^2 \ln R_1 - R_1^2 \ln R_2}, \quad (56)$$

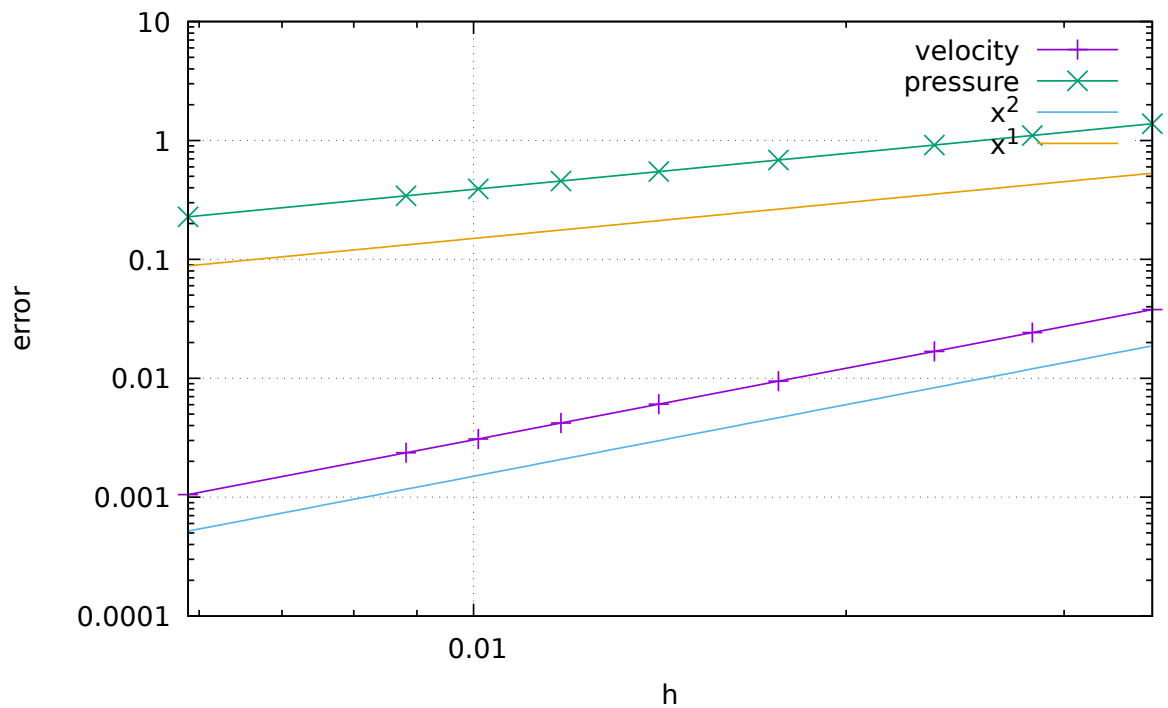
$$B = -C \frac{R_2^2 - R_1^2}{R_2^2 \ln R_1 - R_1^2 \ln R_2}. \quad (57)$$

The parameters  $A$  and  $B$  are chosen so that  $v_r(R_1) = v_r(R_2) = 0$ , i.e. the velocity is tangential to both inner and outer surfaces. The gravity vector is radial and of unit length. In the present case, we set  $R_1 = 1$ ,  $R_2 = 2$  and  $C = -1$ .

### features

- $Q_1 \times P_0$  element
- incompressible flow
- penalty formulation
- Dirichlet boundary conditions
- direct solver
- isothermal
- isoviscous
- analytical solution
- annulus geometry
- elemental boundary conditions

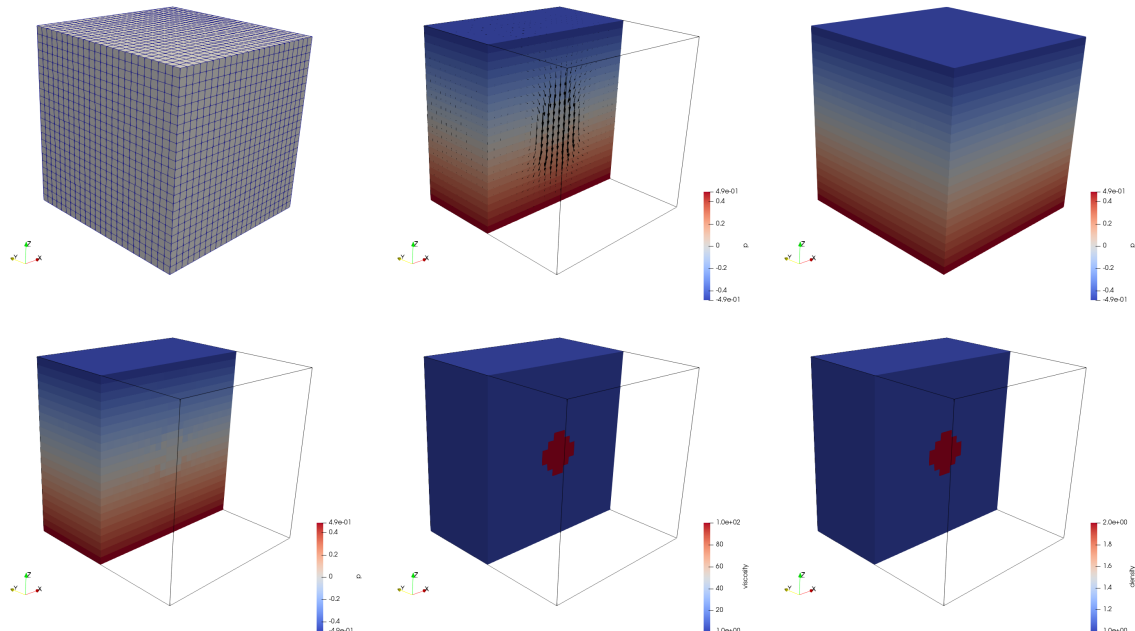




## 13 fieldstone: stokes sphere (3D) - penalty

### features

- $Q_1 \times P_0$  element
- incompressible flow
- penalty formulation
- Dirichlet boundary conditions (free-slip)
- direct solver
- isothermal
- non-isoviscous
- 3D
- elemental b.c.
- buoyancy driven



## 14 fieldstone: stokes sphere (3D) - mixed formulation

This is the same setup as Section 14.

### features

- $Q_1 \times P_0$  element
- incompressible flow
- mixed formulation
- Dirichlet boundary conditions (free-slip)
- direct solver
- isothermal
- non-isoviscous
- 3D
- elemental b.c.
- buoyancy driven

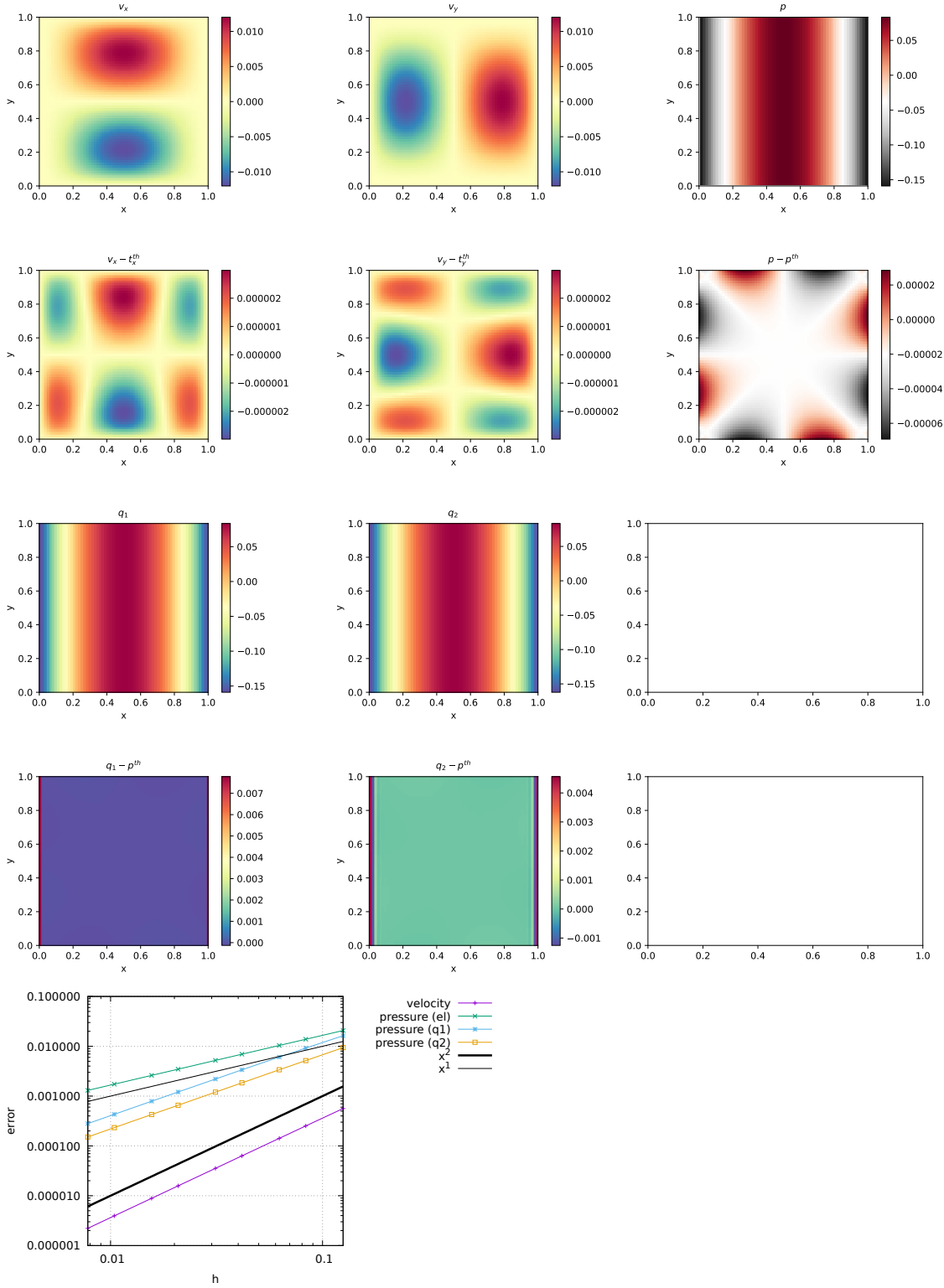
## 15 fieldstone: consistent pressure recovery

$$p = -\lambda \nabla \cdot \mathbf{v}$$

$q_1$  is smoothed pressure obtained with the center-to-node approach.

$q_2$  is recovered pressure obtained with [58].

All three fulfill the zero average condition:  $\int p d\Omega = 0$ .



In terms of pressure error,  $q_2$  is better than  $q_1$  which is better than elemental.

QUESTION: why are the averages exactly zero ?!

TODO:

- add randomness to internal node positions.
- look at elefant algorithms

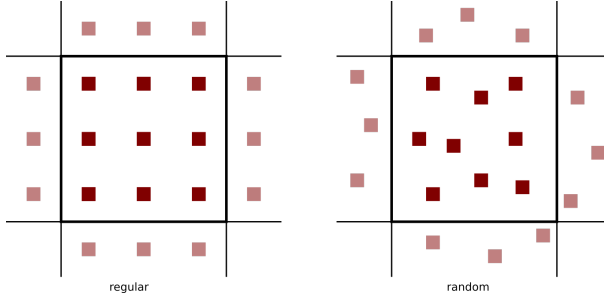
## 16 fieldstone: the Particle in Cell technique (1) - the effect of averaging

### features

- $Q_1 \times P_0$  element
- incompressible flow
- penalty formulation
- Dirichlet boundary conditions (no-slip)
- isothermal
- non-isoviscous
- particle-in-cell

After the initial setup of the grid, markers can then be generated and placed in the domain. One could simply randomly generate the marker positions in the whole domain but unless a *very* large number of markers is used, the chance that an element does not contain any marker exists and this will prove problematic. In order to get a better control over the markers spatial distribution, one usually generates the marker per element, so that the total number of markers in the domain is the product of the number of elements times the user-chosen initial number of markers per element.

Our next concern is how to actually place the markers inside an element. Two methods come to mind: on a regular grid, or in a random manner, as shown on the following figure:



In both cases we make use of the basis shape functions: we generate the positions of the markers (random or regular) in the reference element first ( $r_{im}, s_{im}$ ), and then map those out to the real element as follows:

$$x_{im} = \sum_i^m N_i(r_{im}, s_{im}) x_i \quad y_{im} = \sum_i^m N_i(r_{im}, s_{im}) y_i$$

where  $x_i, y_i$  are the coordinates of the vertices of the element.

When using *active* markers, one is faced with the problem of transferring the properties they carry to the mesh on which the PDEs are to be solved. As we have seen, building the FE matrix involves a loop over all elements, so one simple approach consists of assigning each element a single property computed as the average of the values carried by the markers in that element. Often in colloquial language "average" refers to the arithmetic mean:

$$\langle \phi \rangle_{am} = \frac{1}{n} \sum_k^n \phi_i$$

where  $\langle \phi \rangle_{am}$  is the arithmetic average of the  $n$  numbers  $\phi_i$ . However, in mathematics other means are commonly used, such as the geometric mean:

$$\langle \phi \rangle_{gm} = \left( \prod_i^n \phi_i \right)$$

and the harmonic mean:

$$\langle \phi \rangle_{hm} = \left( \frac{1}{n} \sum_i^n \frac{1}{\phi_i} \right)^{-1}$$

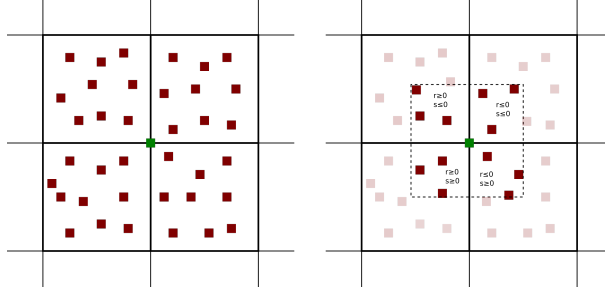
Furthermore, there is a well known inequality for any set of positive numbers,

$$\langle \phi \rangle_{am} \geq \langle \phi \rangle_{gm} \geq \langle \phi \rangle_{hm}$$

which will prove to be important later on.

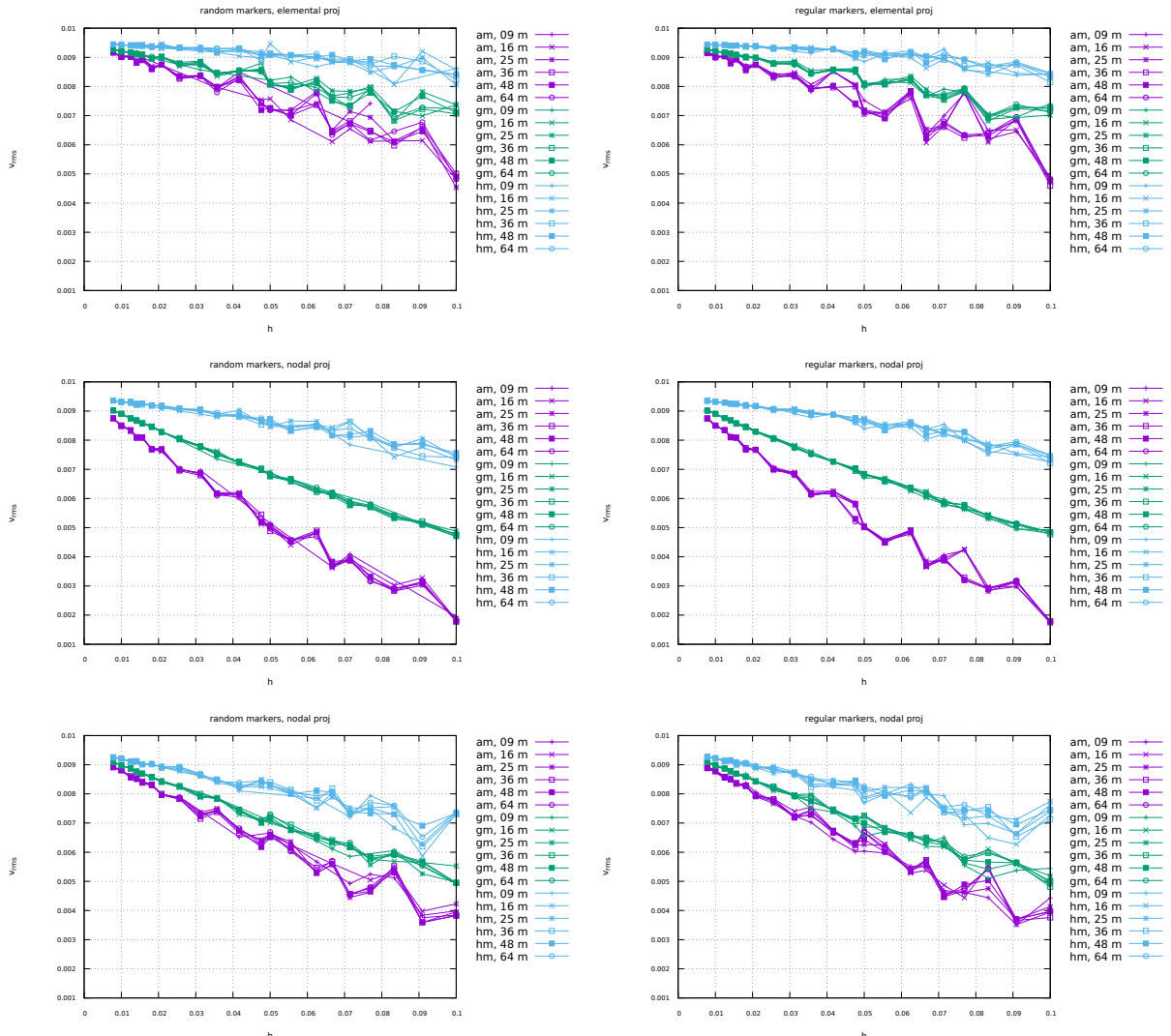
Let us now turn to a simple concrete example: the 2D Stokes sphere. There are two materials in the domain, so that markers carry the label "mat=1" or "mat=2". For each element an average density and viscosity need to be computed. The majority of elements contains markers with a single material label so that the choice of averaging does not matter (it is trivial to verify that if  $\phi_i = \phi_0$  then  $\langle \phi \rangle_{am} = \langle \phi \rangle_{gm} = \langle \phi \rangle_{hm} = \phi_0$ ). Remain the elements crossed by the interface between the two materials: they contain markers of both materials and the average density and viscosity inside those depends on 1) the total number of markers inside the element, 2) the ratio of markers 1 to markers 2, 3) the type of averaging.

This averaging problem has been studied and documented in the literature [45, 13, 52, 41]



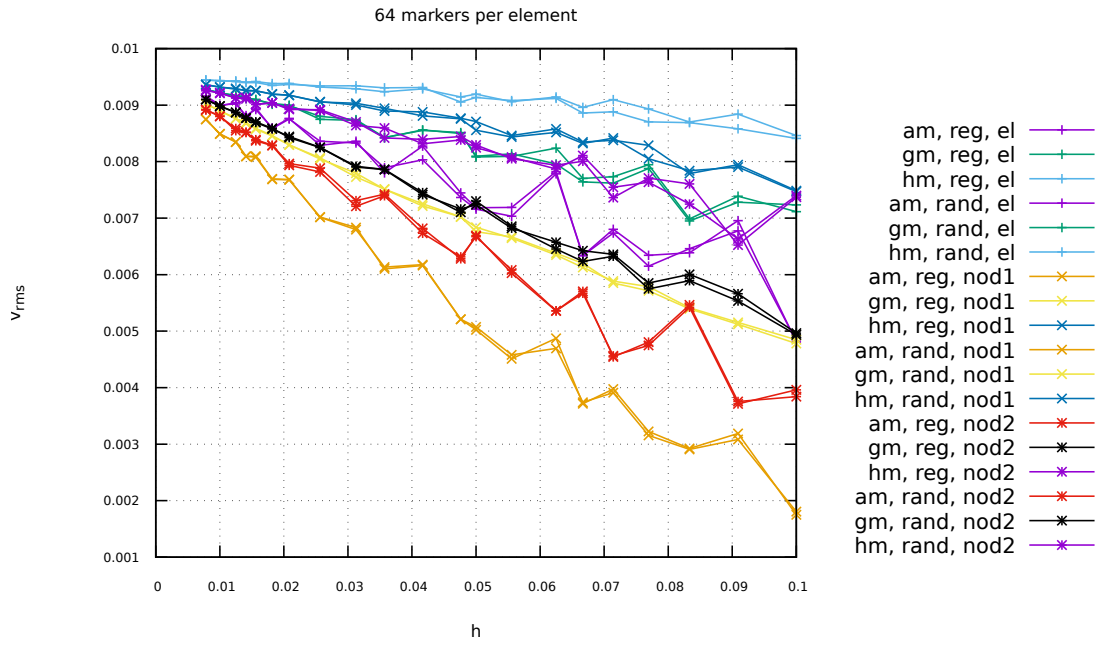
Nodal projection. Left: all markers inside elements to which the green node belongs to are taken into account.  
Right: only the markers closest to the green node count.

The setup is identical as the Stokes sphere experiment. The bash script *runall* runs the code for many resolutions, both initial marker distribution and all three averaging types. The viscosity of the sphere has been set to  $10^3$  while the viscosity of the surrounding fluid is 1. The average density is always computed with an arithmetic mean. Root mean square velocity results are shown hereunder:



## Conclusions:

- With increasing resolution ( $h \rightarrow 0$ ) vrms values seem to converge towards a single value, irrespective of the number of markers.
- At low resolution, say 32x32 (i.e.  $h=0.03125$ ), vrms values for the three averagings differ by about 10%. At higher resolution, say 128x128, vrms values are still not converged.
- The number of markers per element plays a role at low resolution, but less and less with increasing resolution.
- Results for random and regular marker distributions are not identical but follow a similar trend and seem to converge to the same value.
- At low resolutions, elemental values yield better results.
- harmonic mean yields overall the best results



## 17 fieldstone: solving the full saddle point problem

The details of the numerical setup are presented in Section 5.

The main difference is that we no longer use the penalty formulation and therefore keep both velocity and pressure as unknowns. Therefore we end up having to solve the following system:

$$\begin{pmatrix} \mathbb{K} & \mathbb{G} \\ \mathbb{G}^T & 0 \end{pmatrix} \cdot \begin{pmatrix} V \\ P \end{pmatrix} = \begin{pmatrix} f \\ h \end{pmatrix} \quad \text{or,} \quad \mathbb{A} \cdot X = rhs$$

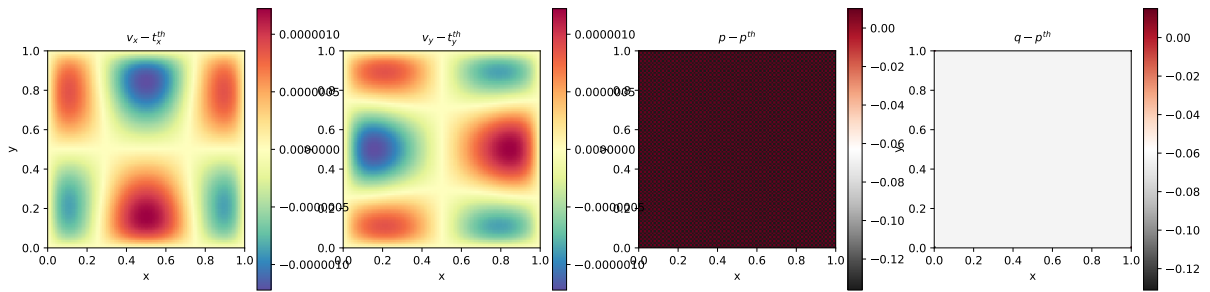
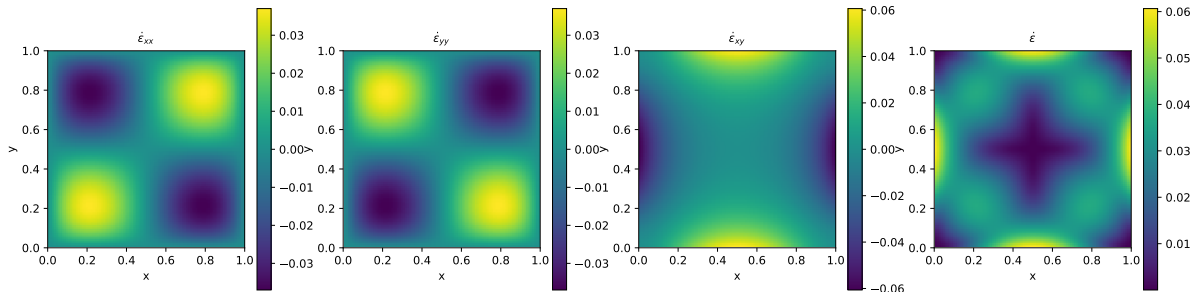
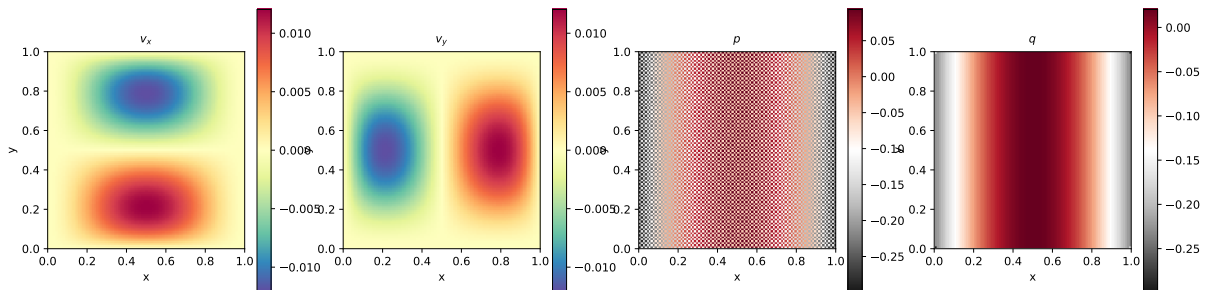
Each block  $\mathbb{K}$ ,  $\mathbb{G}$  and vector  $f$ ,  $h$  are built separately in the code and assembled into the matrix  $\mathbb{A}$  and vector  $rhs$  afterwards.  $\mathbb{A}$  and  $rhs$  are then passed to the solver. We will see later that there are alternatives to solve this approach which do not require to build the full Stokes matrix  $\mathbb{A}$ .

Each element has  $m = 4$  vertices so in total  $ndofV \times m = 8$  velocity dofs and a single pressure dof, commonly situated in the center of the element. The total number of velocity dofs is therefore  $NfemV = nnp \times ndofV$  while the total number of pressure dofs is  $NfemP = nel$ . The total number of dofs is then  $Nfem = NfemV + NfemP$ .

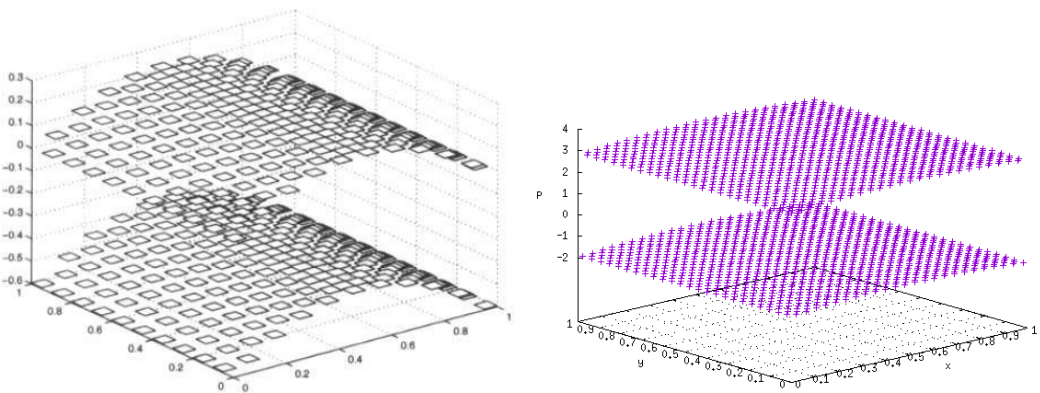
As a consequence, matrix  $\mathbb{K}$  has size  $NfemV, NfemV$  and matrix  $\mathbb{G}$  has size  $NfemV, NfemP$ . Vector  $f$  is of size  $NfemV$  and vector  $h$  is of size  $NfemP$ .

### features

- $Q_1 \times P_0$  element
- incompressible flow
- mixed formulation
- Dirichlet boundary conditions (no-slip)
- direct solver (?)
- isothermal
- isoviscous
- analytical solution
- pressure smoothing



Unlike the results obtained with the penalty formualtion (see Section 5), the pressure showcases a very strong checkerboard pattern, similar to the one in [16].



Left: pressure solution as shown in [16]; Right: pressure solution obtained with fieldstone.

Rather interestingly, the nodal pressure (obtained with a simple center-to-node algorithm) fails to recover a correct pressure at the four corners.

## 18 fieldstone: solving the full saddle point problem in 3D

this does not work because of the Dirichlet b.c. on all 6 sides and all three components It does work well with Q2Q1.

This benchmark begins by postulating a polynomial solution to the 3D Stokes equation [14]:

$$\mathbf{v} = \begin{pmatrix} x + x^2 + xy + x^3y \\ y + xy + y^2 + x^2y^2 \\ -2z - 3xz - 3yz - 5x^2yz \end{pmatrix} \quad (58)$$

and

$$p = xyz + x^3y^3z - 5/32 \quad (59)$$

While it is then trivial to verify that this velocity field is divergence-free, the corresponding body force of the Stokes equation can be computed by inserting this solution into the momentum equation with a given viscosity  $\mu$  (constant or position/velocity/strain rate dependent). The domain is a unit cube and velocity boundary conditions simply use Eq. (58). Following [7], the viscosity is given by the smoothly varying function

$$\mu = \exp(1 - \beta(x(1-x) + y(1-y) + z(1-z))) \quad (60)$$

Choosing  $\beta = 0$  yields a constant velocity  $\mu = e^1$  (and greatly simplifies the right-hand side). One can easily show that the ratio of viscosities  $\mu^*$  in the system follows  $\mu^* = \exp(-3\beta/4)$  so that choosing  $\beta = 10$  yields  $\mu^* \simeq 1808$  and  $\beta = 20$  yields  $\mu^* \simeq 3.269 \times 10^6$ .

We start from the momentum conservation equation:

$$-\nabla p + \nabla \cdot (2\mu \dot{\epsilon}) = \mathbf{f}$$

The  $x$ -component of this equation writes

$$f_x = -\frac{\partial p}{\partial x} + \frac{\partial}{\partial x}(2\mu \dot{\epsilon}_{xx}) + \frac{\partial}{\partial y}(2\mu \dot{\epsilon}_{xy}) + \frac{\partial}{\partial z}(2\mu \dot{\epsilon}_{xz}) \quad (61)$$

$$= -\frac{\partial p}{\partial x} + 2\mu \frac{\partial}{\partial x} \dot{\epsilon}_{xx} + 2\mu \frac{\partial}{\partial y} \dot{\epsilon}_{xy} + 2\mu \frac{\partial}{\partial z} \dot{\epsilon}_{xz} + 2\frac{\partial \mu}{\partial x} \dot{\epsilon}_{xx} + 2\frac{\partial \mu}{\partial y} \dot{\epsilon}_{xy} + 2\frac{\partial \mu}{\partial z} \dot{\epsilon}_{xz} \quad (62)$$

Let us compute all the block separately:

$$\begin{aligned} \dot{\epsilon}_{xx} &= 1 + 2x + y + 3x^2y \\ \dot{\epsilon}_{yy} &= 1 + x + 2y + 2x^2y \\ \dot{\epsilon}_{zz} &= -2 - 3x - 3y - 5x^2y \\ 2\dot{\epsilon}_{xy} &= (x + x^3) + (y + 2xy^2) = x + y + 2xy^2 + x^3 \\ 2\dot{\epsilon}_{xz} &= (0) + (-3z - 10xyz) = -3z - 10xyz \\ 2\dot{\epsilon}_{yz} &= (0) + (-3z - 5x^2z) = -3z - 5x^2z \end{aligned}$$

In passing, one can verify that  $\dot{\epsilon}_{xx} + \dot{\epsilon}_{yy} + \dot{\epsilon}_{zz} = 0$ . We further have

$$\begin{aligned} \frac{\partial}{\partial x} 2\dot{\epsilon}_{xx} &= 2(2 + 6xy) \\ \frac{\partial}{\partial y} 2\dot{\epsilon}_{xy} &= 1 + 4xy \\ \frac{\partial}{\partial z} 2\dot{\epsilon}_{xz} &= -3 - 10xy \\ \frac{\partial}{\partial x} 2\dot{\epsilon}_{xy} &= 1 + 2y^2 + 3x^2 \\ \frac{\partial}{\partial y} 2\dot{\epsilon}_{yy} &= 2(2 + 2x^2) \\ \frac{\partial}{\partial z} 2\dot{\epsilon}_{yz} &= -3 - 5x^2 \\ \frac{\partial}{\partial x} 2\dot{\epsilon}_{xz} &= -10yz \\ \frac{\partial}{\partial y} 2\dot{\epsilon}_{yz} &= 0 \\ \frac{\partial}{\partial z} 2\dot{\epsilon}_{zz} &= 2(0) \end{aligned}$$

$$\frac{\partial p}{\partial x} = yz + 3x^2y^3z \quad (63)$$

$$\frac{\partial p}{\partial y} = xz + 3x^3y^2z \quad (64)$$

$$\frac{\partial p}{\partial z} = xy + x^3y^3 \quad (65)$$

The viscosity is chosen to be

$$\mu(x, y, z) = \exp [1 - \beta(x(1-x) + y(1-y) + z(1-z))]$$

**Constant viscosity** Setting  $\beta = 0$  yields

$$\mu(x, y, z) = e \simeq 2.718$$

so that

$$\frac{\partial}{\partial x} \mu(x, y, z) = 0 \quad (66)$$

$$\frac{\partial}{\partial y} \mu(x, y, z) = 0 \quad (67)$$

$$\frac{\partial}{\partial z} \mu(x, y, z) = 0 \quad (68)$$

and

$$\begin{aligned} f_x &= -\frac{\partial p}{\partial x} + 2\mu \frac{\partial}{\partial x} \dot{\epsilon}_{xx} + 2\mu \frac{\partial}{\partial y} \dot{\epsilon}_{xy} + 2\mu \frac{\partial}{\partial z} \dot{\epsilon}_{xz} \\ &= -(yz + 3x^2y^3z) + 2(2 + 6xy) + (1 + 4xy) + (-3 - 10xy) \end{aligned} \quad (69)$$

$$= -(yz + 3x^2y^3z) + \mu(2 + 6xy) \quad (70)$$

$$\begin{aligned} f_y &= -\frac{\partial p}{\partial y} + 2\mu \frac{\partial}{\partial x} \dot{\epsilon}_{xy} + 2\mu \frac{\partial}{\partial y} \dot{\epsilon}_{yy} + 2\mu \frac{\partial}{\partial z} \dot{\epsilon}_{yz} \\ &= -(xz + 3x^3y^2z) + \mu(1 + 2y^2 + 3x^2) + \mu 2(2 + 2x^2) + \mu(-3 - 5x^2) \end{aligned} \quad (71)$$

$$= -(xz + 3x^3y^2z) + \mu(2 + 2x^2 + 2y^2) \quad (72)$$

$$\begin{aligned} f_z &= -\frac{\partial p}{\partial z} + 2\mu \frac{\partial}{\partial x} \dot{\epsilon}_{xz} + 2\mu \frac{\partial}{\partial y} \dot{\epsilon}_{yz} + 2\mu \frac{\partial}{\partial z} \dot{\epsilon}_{zz} \\ &= -(xy + x^3y^3) + \mu(-10yz) + 0 + 0 \end{aligned} \quad (73)$$

$$= -(xy + x^3y^3) + \mu(-10yz) \quad (74)$$

finally

$$\mathbf{f} = - \begin{pmatrix} yz + 3x^2y^3z \\ xz + 3x^3y^2z \\ xy + x^3y^3 \end{pmatrix} + \mu \begin{pmatrix} 2 + 6xy \\ 2 + 2x^2 + 2y^2 \\ -10yz \end{pmatrix}$$

$\Rightarrow$  sign problem with Burstedde et al Eq 26 !!

**Variable viscosity**

$$\begin{aligned} \frac{\partial}{\partial x} \mu(x, y, z) &= -(1 - 2x)\beta\mu(x, y, z) \\ \frac{\partial}{\partial y} \mu(x, y, z) &= -(1 - 2y)\beta\mu(x, y, z) \\ \frac{\partial}{\partial z} \mu(x, y, z) &= -(1 - 2z)\beta\mu(x, y, z) \end{aligned}$$

$$\begin{aligned}
\mathbf{f} &= - \begin{pmatrix} yz + 3x^2y^3z \\ xz + 3x^3y^2z \\ xy + x^3y^3 \end{pmatrix} + \mu \begin{pmatrix} 2 + 6xy \\ 2 + 2x^2 + 2y^2 \\ -10yz \end{pmatrix} \\
&\quad - (1 - 2x)\beta\mu(x, y, z) \begin{pmatrix} 2\dot{\epsilon}_{xx} \\ 2\dot{\epsilon}_{xy} \\ 2\dot{\epsilon}_{xz} \end{pmatrix} - (1 - 2y)\beta\mu(x, y, z) \begin{pmatrix} 2\dot{\epsilon}_{xy} \\ 2\dot{\epsilon}_{yy} \\ 2\dot{\epsilon}_{yz} \end{pmatrix} - (1 - 2z)\beta\mu(x, y, z) \begin{pmatrix} 2\dot{\epsilon}_{xz} \\ 2\dot{\epsilon}_{yz} \\ 2\dot{\epsilon}_{zz} \end{pmatrix} \\
&= - \begin{pmatrix} yz + 3x^2y^3z \\ xz + 3x^3y^2z \\ xy + x^3y^3 \end{pmatrix} + \mu \begin{pmatrix} 2 + 6xy \\ 2 + 2x^2 + 2y^2 \\ -10yz \end{pmatrix} \\
&\quad - (1 - 2x)\beta\mu \begin{pmatrix} 2 + 4x + 2y + 6x^2y \\ x + y + 2xy^2 + x^3 \\ -3z - 10xyz \end{pmatrix} - (1 - 2y)\beta\mu \begin{pmatrix} x + y + 2xy^2 + x^3 \\ 2 + 2x + 4y + 4x^2y \\ -3z - 5x^2z \end{pmatrix} - (1 - 2z)\beta\mu \begin{pmatrix} -3z - 10xyz \\ -3z - 5x^2z \\ -4 - 6x - 6y - 10x^2y \end{pmatrix}
\end{aligned} \tag{75}$$

at  $(x, y, z) = (0, 0, 0)$ ,  $\mu = \exp(1)$ ,

at  $(x, y, z) = (0.5, 0.5, 0.5)$ ,  $\mu = \exp(1 - 3\beta/4)$

Viscosity ratio is given by

$$\mu^* = \frac{\exp(1 - 3\beta/4)}{\exp(1)} = \exp(-3\beta/4)$$

By varying  $\beta$  between 1 and 22 we can get up to 7 orders of magnitude viscosity difference !

#### features

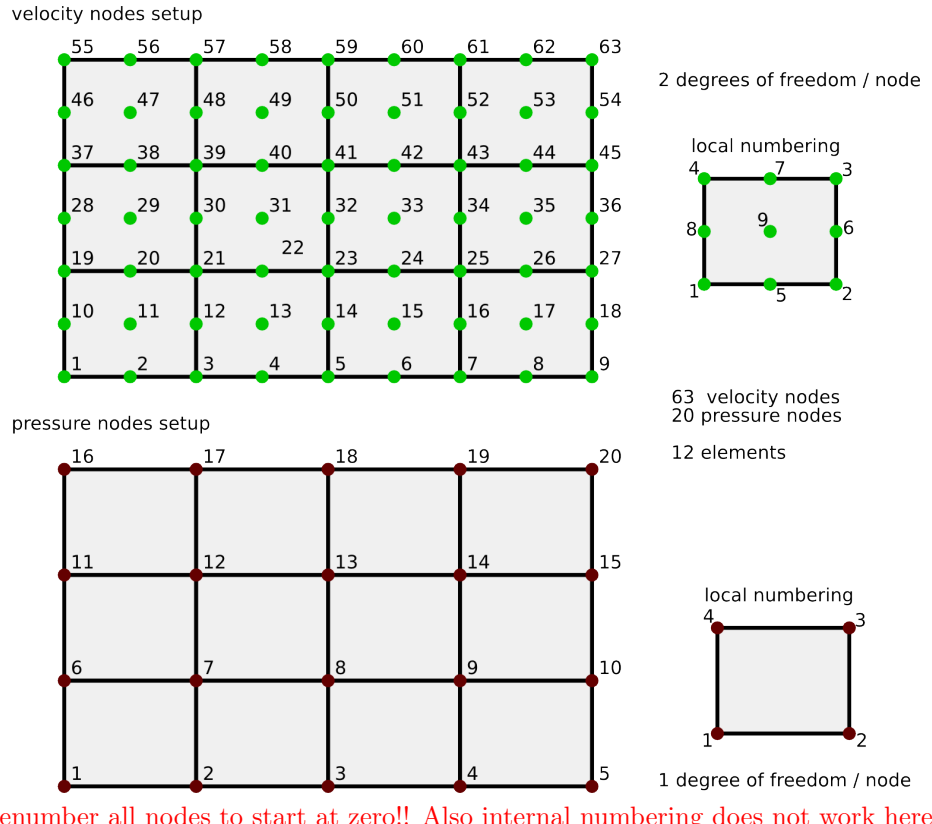
- $Q_1 \times P_0$  element
- incompressible flow
- saddle point system
- Dirichlet boundary conditions (free-slip)
- direct solver
- isothermal
- non-isoviscous
- 3D
- elemental b.c.
- analytical solution

## 19 fieldstone: solving the full saddle point problem with $Q_2 \times Q_1$ elements

The details of the numerical setup are presented in Section 5.

Each element has  $m_V = 9$  vertices so in total  $ndof_V \times m_V = 18$  velocity dofs and  $ndof_P \times m_P = 4$  pressure dofs. The total number of velocity dofs is therefore  $NfemV = nnp \times ndofV$  while the total number of pressure dofs is  $NfemP = nel$ . The total number of dofs is then  $Nfem = NfemV + NfemP$ .

As a consequence, matrix  $\mathbb{K}$  has size  $NfemV, NfemV$  and matrix  $\mathbb{G}$  has size  $NfemV, NfemP$ . Vector  $f$  is of size  $NfemV$  and vector  $h$  is of size  $NfemP$ .

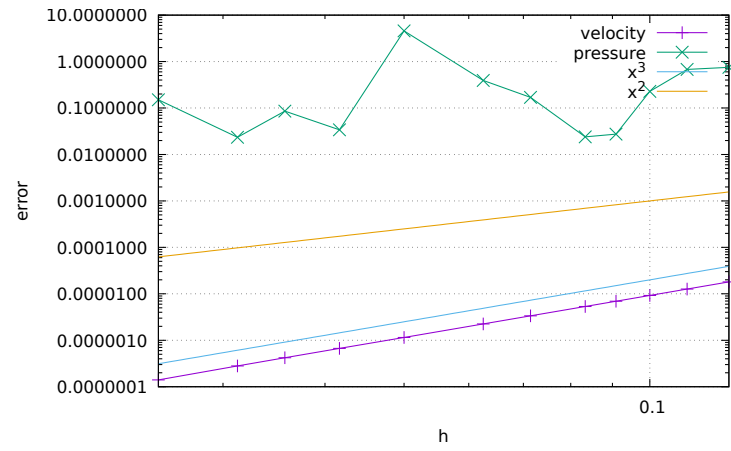


ToDo:

- normalise pressure

### features

- $Q_2 \times Q_1$  element
- incompressible flow
- mixed formulation
- Dirichlet boundary conditions (no-slip)
- isothermal
- isoviscous
- analytical solution

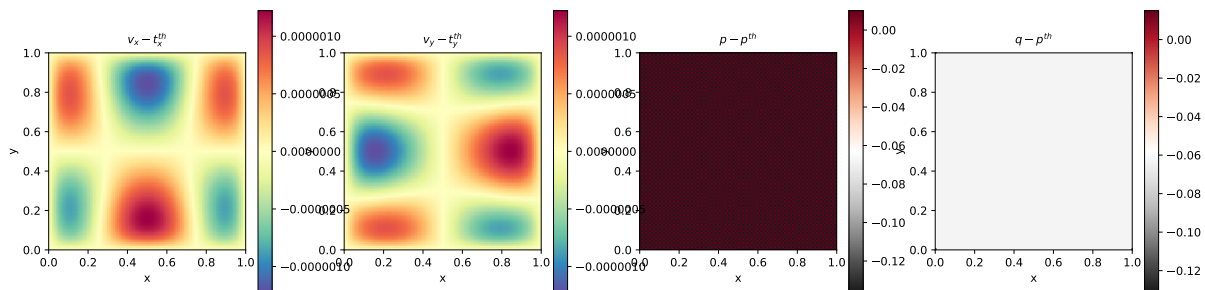
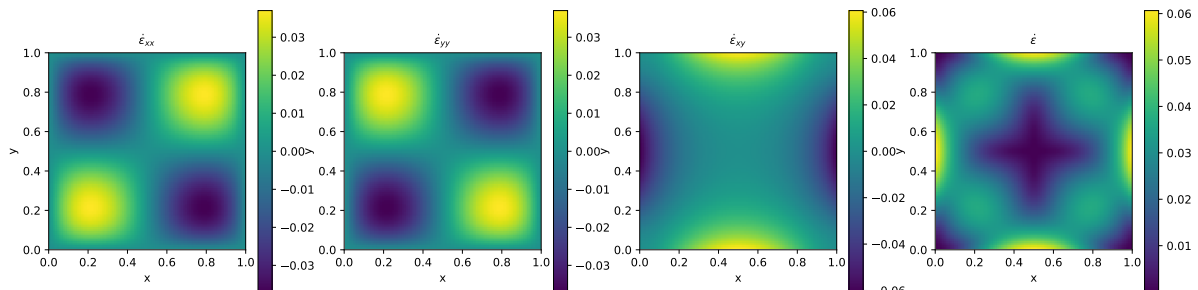
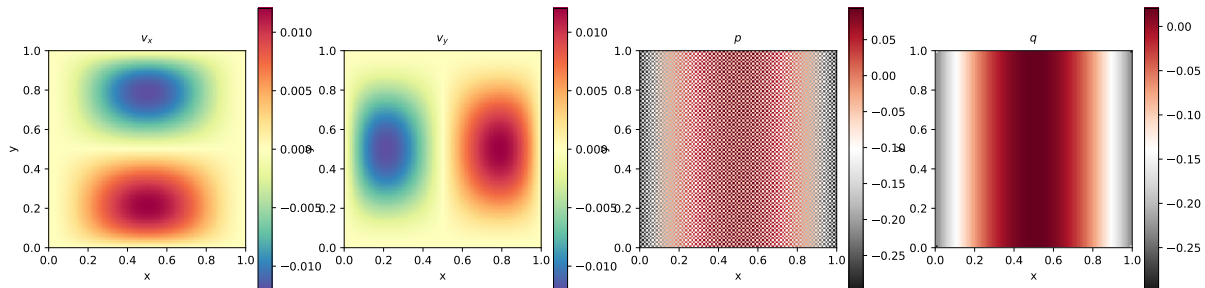


## 20 fieldstone: The non-conforming $Q_1 \times P_0$ element

### features

- Non-conforming  $Q_1 \times P_0$  element
- incompressible flow
- mixed formulation
- isothermal
- non-isoviscous
- analytical solution
- pressure smoothing

try Q1 mapping instead of isoparametric.



## **21 fieldstone: The stabilised $Q_1 \times Q_1$ element**

The details of the numerical setup are presented in Section 5.

## 22 fieldstone: compressible flow (1)

We first start with an isothermal Stokes flow, so that we disregard the heat transport equation and the equations we wish to solve are simply:

$$-\nabla \cdot \left[ 2\eta \left( \dot{\varepsilon}(\mathbf{v}) - \frac{1}{3}(\nabla \cdot \mathbf{v})\mathbf{1} \right) \right] + \nabla p = \rho \mathbf{g} \quad \text{in } \Omega, \quad (76)$$

$$\nabla \cdot (\rho \mathbf{v}) = 0 \quad \text{in } \Omega \quad (77)$$

The second equation can be rewritten  $\nabla \cdot (\rho \mathbf{v}) = \rho \nabla \cdot \mathbf{v} + \mathbf{v} \cdot \nabla \rho = 0$  or,

$$\nabla \cdot \mathbf{v} + \frac{1}{\rho} \mathbf{v} \cdot \nabla \rho = 0$$

Note that this presupposes that the density is not zero anywhere in the domain.

We use a mixed formulation and therefore keep both velocity and pressure as unknowns. We end up having to solve the following system:

$$\begin{pmatrix} \mathbb{K} & \mathbb{G} \\ \mathbb{G}^T + \mathbb{Z} & 0 \end{pmatrix} \cdot \begin{pmatrix} \mathcal{V} \\ \mathcal{P} \end{pmatrix} = \begin{pmatrix} f \\ h \end{pmatrix} \quad \text{or,} \quad \mathbb{A} \cdot X = rhs$$

Where  $\mathbb{K}$  is the stiffness matrix,  $\mathbb{G}$  is the discrete gradient operator,  $\mathbb{G}^T$  is the discrete divergence operator,  $\mathcal{V}$  the velocity vector,  $\mathcal{P}$  the pressure vector. Note that the term  $\mathbb{Z}\mathcal{V}$  derives from term  $\mathbf{v} \cdot \nabla \rho$  in the continuity equation.

Each block  $\mathbb{K}$ ,  $\mathbb{G}$ ,  $\mathbb{Z}$  and vectors  $f$  and  $h$  are built separately in the code and assembled into the matrix  $\mathbb{A}$  and vector  $rhs$  afterwards.  $\mathbb{A}$  and  $rhs$  are then passed to the solver. We will see later that there are alternatives to solve this approach which do not require to build the full Stokes matrix  $\mathbb{A}$ .

*Remark:* the term  $\mathbb{Z}\mathcal{V}$  is often put in the rhs (i.e. added to  $h$ ) so that the matrix  $\mathbb{A}$  retains the same structure as in the incompressible case. This is indeed how it is implemented in ASPECT. This however requires more work since the rhs depends on the solution and some form of iterations is needed.

In the case of a compressible flow the strain rate tensor and the deviatoric strain rate tensor are no more equal (since  $\nabla \cdot \mathbf{v} \neq 0$ ). The deviatoric strainrate tensor is given by<sup>2</sup>

$$\dot{\epsilon}^d(\mathbf{v}) = \dot{\epsilon}(\mathbf{v}) - \frac{1}{3} Tr(\dot{\epsilon})\mathbf{1} = \dot{\epsilon}(\mathbf{v}) - \frac{1}{3}(\nabla \cdot \mathbf{v})\mathbf{1}$$

In that case:

$$\dot{\epsilon}_{xx}^d = \frac{\partial u}{\partial x} - \frac{1}{3} \left( \frac{\partial u}{\partial x} + \frac{\partial v}{\partial y} \right) = \frac{2}{3} \frac{\partial u}{\partial x} - \frac{1}{3} \frac{\partial v}{\partial y} \quad (78)$$

$$\dot{\epsilon}_{yy}^d = \frac{\partial v}{\partial y} - \frac{1}{3} \left( \frac{\partial u}{\partial x} + \frac{\partial v}{\partial y} \right) = -\frac{1}{3} \frac{\partial u}{\partial x} + \frac{2}{3} \frac{\partial v}{\partial y} \quad (79)$$

$$2\dot{\epsilon}_{xy}^d = \frac{\partial u}{\partial y} + \frac{\partial v}{\partial x} \quad (80)$$

and then

$$\dot{\epsilon}^d(\mathbf{v}) = \begin{pmatrix} \frac{2}{3} \frac{\partial u}{\partial x} - \frac{1}{3} \frac{\partial v}{\partial y} & \frac{1}{2} \frac{\partial u}{\partial y} + \frac{1}{2} \frac{\partial v}{\partial x} \\ \frac{1}{2} \frac{\partial u}{\partial y} + \frac{1}{2} \frac{\partial v}{\partial x} & -\frac{1}{3} \frac{\partial u}{\partial x} + \frac{2}{3} \frac{\partial v}{\partial y} \end{pmatrix}$$

From  $\vec{\tau} = 2\eta \vec{\epsilon}^d$  we arrive at:

$$\begin{pmatrix} \tau_{xx} \\ \tau_{yy} \\ \tau_{xy} \end{pmatrix} = 2\eta \begin{pmatrix} \dot{\epsilon}_{xx}^d \\ \dot{\epsilon}_{yy}^d \\ \dot{\epsilon}_{xy}^d \end{pmatrix} = 2\eta \begin{pmatrix} 2/3 & -1/3 & 0 \\ -1/3 & 2/3 & 0 \\ 0 & 0 & 1/2 \end{pmatrix} \cdot \begin{pmatrix} \frac{\partial u}{\partial x} \\ \frac{\partial v}{\partial y} \\ \frac{\partial u}{\partial y} + \frac{\partial v}{\partial x} \end{pmatrix} = \eta \begin{pmatrix} 4/3 & -2/3 & 0 \\ -2/3 & 4/3 & 0 \\ 0 & 0 & 1 \end{pmatrix} \cdot \begin{pmatrix} \frac{\partial u}{\partial x} \\ \frac{\partial v}{\partial y} \\ \frac{\partial u}{\partial y} + \frac{\partial v}{\partial x} \end{pmatrix}$$

or,

$$\vec{\tau} = \mathbf{C}_\eta \mathbf{B} \mathbf{V}$$

---

<sup>2</sup>See the ASPECT manual for a justification of the 3 value in the denominator in 2D and 3D.

In order to test our implementation we have created a few manufactured solutions:

- benchmark #1 (ibench=1): Starting from a density profile of:

$$\rho(x, y) = xy \quad (81)$$

We derive a velocity given by:

$$v_x(x, y) = \frac{C_x}{x}, v_y(x, y) = \frac{C_y}{y} \quad (82)$$

With  $g_x(x, y) = \frac{1}{x}$  and  $g_y(x, y) = \frac{1}{y}$ , this leads us to a pressure profile:

$$p = -\eta \left( \frac{4C_x}{3x^2} + \frac{4C_y}{3y^2} \right) + xy + C_0 \quad (83)$$

This gives us a strain rate:

$$\dot{\epsilon}_{xx} = \frac{-C_x}{x^2} \quad \dot{\epsilon}_{yy} = \frac{-C_y}{y^2} \quad \dot{\epsilon}_{xy} = 0$$

In what follows, we choose  $\eta = 1$  and  $C_x = C_y = 1$  and for a unit square domain  $[1 : 2] \times [1 : 2]$  we compute  $C_0$  so that the pressure is normalised to zero over the whole domain and obtain  $C_0 = -1$ .

- benchmark #2 (ibench=2): Starting from a density profile of:

$$\rho = \cos(x) \cos(y) \quad (84)$$

We derive a velocity given by:

$$v_x = \frac{C_x}{\cos(x)}, v_y = \frac{C_y}{\cos(y)} \quad (85)$$

With  $g_x = \frac{1}{\cos(y)}$  and  $g_y = \frac{1}{\cos(x)}$ , this leads us to a pressure profile:

$$\begin{aligned} p &= \eta \left( \frac{4C_x \sin(x)}{3 \cos^2(x)} + \frac{4C_y \sin(y)}{3 \cos^2(y)} \right) + (\sin(x) + \sin(y)) + C_0 \\ \dot{\epsilon}_{xx} &= C_x \frac{\sin(x)}{\cos^2(x)} \quad \dot{\epsilon}_{yy} = C_y \frac{\sin(y)}{\cos^2(y)} \quad \dot{\epsilon}_{xy} = 0 \end{aligned} \quad (86)$$

We choose  $\eta = 1$  and  $C_x = C_y = 1$ . The domain is the unit square  $[0 : 1] \times [0 : 1]$  and we obtain  $C_0$  as before and obtain

$$C_0 = 2 - 2 \cos(1) + 8/3(\frac{1}{\cos(1)} - 1) \simeq 3.18823730$$

(thank you WolframAlpha)

- benchmark #3 (ibench=3)
- benchmark #4 (ibench=4)
- benchmark #5 (ibench=5)

## features

- $Q_1 \times P_0$  element
- incompressible flow
- mixed formulation
- Dirichlet boundary conditions (no-slip)
- isothermal
- isoviscous
- analytical solution
- pressure smoothing

ToDo:

- pbs with odd vs even number of elements
- q is 'fine' everywhere except in the corners - revisit pressure smoothing paper?
- redo A v d Berg benchmark (see Tom Weir thesis)

## 23 fieldstone: compressible flow (2)

### 23.1 The physics

Let us start with some thermodynamics. Every material has an equation of state. The equilibrium thermodynamic state of any material can be constrained if any two state variables are specified. Examples of state variables include the pressure  $p$  and specific volume  $\nu = 1/\rho$ , as well as the temperature  $T$ .

After linearisation, the density depends on temperature and pressure as follows:

$$\rho(T, p) = \rho_0 ((1 - \alpha(T - T_0)) + \beta_T p)$$

where  $\alpha$  is the coefficient of thermal expansion, also called thermal expansivity:

$$\alpha = -\frac{1}{\rho} \left( \frac{\partial \rho}{\partial T} \right)_p$$

$\alpha$  is the percentage increase in volume of a material per degree of temperature increase; the subscript  $p$  means that the pressure is held fixed.

$\beta_T$  is the isothermal compressibility of the fluid, which is given by

$$\beta_T = \frac{1}{K} = \frac{1}{\rho} \left( \frac{\partial \rho}{\partial P} \right)_T$$

with  $K$  the bulk modulus. Values of  $\beta_T = 10^{-12} - 10^{-11} \text{ Pa}^{-1}$  are reasonable for Earth's mantle, with values decreasing by about a factor of 5 between the shallow lithosphere and core-mantle boundary. This is the percentage increase in density per unit change in pressure at constant temperature. Both the coefficient of thermal expansion and the isothermal compressibility can be obtained from the equation of state.

The full set of equations we wish to solve is given by

$$-\nabla \cdot [2\eta \dot{\epsilon}^d(\mathbf{v})] + \nabla p = \rho_0 ((1 - \alpha(T - T_0)) + \beta_T p) \mathbf{g} \quad \text{in } \Omega \quad (87)$$

$$\nabla \cdot \mathbf{v} + \frac{1}{\rho} \mathbf{v} \cdot \nabla \rho = 0 \quad \text{in } \Omega \quad (88)$$

$$\rho C_p \left( \frac{\partial T}{\partial t} + \mathbf{v} \cdot \nabla T \right) - \nabla \cdot k \nabla T = \rho H + 2\eta \dot{\epsilon}^d : \dot{\epsilon}^d + \alpha T \left( \frac{\partial p}{\partial t} + \mathbf{v} \cdot \nabla p \right) \quad \text{in } \Omega, \quad (89)$$

Note that this presupposes that the density is not zero anywhere in the domain.

### 23.2 The numerics

We use a mixed formulation and therefore keep both velocity and pressure as unknowns. We end up having to solve the following system:

$$\begin{pmatrix} \mathbb{K} & \mathbb{G} + \mathbb{W} \\ \mathbb{G}^T + \mathbb{Z} & 0 \end{pmatrix} \cdot \begin{pmatrix} \mathcal{V} \\ \mathcal{P} \end{pmatrix} = \begin{pmatrix} f \\ h \end{pmatrix} \quad \text{or,} \quad \mathbb{A} \cdot X = rhs$$

Where  $\mathbb{K}$  is the stiffness matrix,  $\mathbb{G}$  is the discrete gradient operator,  $\mathbb{G}^T$  is the discrete divergence operator,  $\mathcal{V}$  the velocity vector,  $\mathcal{P}$  the pressure vector. Note that the term  $\mathbb{Z}\mathcal{V}$  derives from term  $\mathbf{v} \cdot \nabla \rho$  in the continuity equation.

As perfectly explained in the step 32 of deal.ii<sup>3</sup>, we need to scale the  $\mathbb{G}$  term since it is many orders of magnitude smaller than  $\mathbb{K}$ , which introduces large inaccuracies in the solving process to the point that the solution is nonsensical. This scaling coefficient is  $\eta/L$ . After building the  $\mathbb{G}$  block, it is then scaled as follows:  $\mathbb{G}' = \frac{\eta}{L} \mathbb{G}$  so that we now solve

$$\begin{pmatrix} \mathbb{K} & \mathbb{G}' + \mathbb{W} \\ \mathbb{G}^T + \mathbb{Z} & 0 \end{pmatrix} \cdot \begin{pmatrix} \mathcal{V} \\ \mathcal{P}' \end{pmatrix} = \begin{pmatrix} f \\ h \end{pmatrix}$$

After the solve phase, we recover the real pressure with  $\mathcal{P} = \frac{\eta}{L} \mathcal{P}'$ .

adapt notes since I should scale  $\mathbb{W}$  and  $\mathbb{Z}$  too.  $\mathcal{h}$  should be caled too !!!!!!!

Each block  $\mathbb{K}$ ,  $\mathbb{G}$ ,  $\mathbb{Z}$  and vectors  $f$  and  $h$  are built separately in the code and assembled into the matrix  $\mathbb{A}$  and vector  $rhs$  afterwards.  $\mathbb{A}$  and  $rhs$  are then passed to the solver. We will see later that there are alternatives to solve this approach which do not require to build the full Stokes matrix  $\mathbb{A}$ .

**Remark 1:** the terms  $\mathbb{Z}\mathcal{V}$  and  $\mathbb{W}\mathcal{P}$  are often put in the rhs (i.e. added to  $h$ ) so that the matrix  $\mathbb{A}$  retains the same structure as in the incompressible case. This is indeed how it is implemented in ASPECT, see also appendix A of [33]. This however requires more work since the rhs depends on the solution and some form of iterations is needed.

---

<sup>3</sup>[https://www.dealii.org/9.0.0/doxygen/deal.II/step\\_32.html](https://www.dealii.org/9.0.0/doxygen/deal.II/step_32.html)

**Remark 2:** Very often the adiabatic heating term  $\alpha T(\mathbf{v} \cdot \nabla p)$  is simplified as follows: If you assume the vertical component of the gradient of the dynamic pressure to be small compared to the gradient of the total pressure (in other words, the gradient is dominated by the gradient of the hydrostatic pressure), then  $-\rho\mathbf{g} \simeq \nabla p$  and then  $\alpha T(\mathbf{v} \cdot \nabla p) \simeq -\alpha\rho T\mathbf{v} \cdot \mathbf{g}$ . We will however not be using this approximation in what follows.

We have already established that

$$\vec{\tau} = \mathbf{C}_\eta \mathbf{B} \mathbf{V}$$

The following measurements are carried out:

- The root mean square velocity (**vrms**):

$$v_{rms} = \sqrt{\frac{1}{V} \int_V v^2 dV}$$

- The average temperature (**Tavg**):

$$\langle T \rangle = \frac{1}{V} \int_V T dV$$

- The total mass (**mass**):

$$M = \int_V \rho dV$$

- The Nusselt number (**Nu**):

$$Nu = -\frac{1}{Lx} \frac{1}{\Delta T} \int_0^{Lx} \frac{\partial T(x, y = L_y)}{\partial y} dx$$

- The kinetic energy (**EK**):

$$E_K = \int_V \frac{1}{2} \rho v^2 dV$$

- The work done against gravity

$$\langle W \rangle = - \int_V \rho g_y v_y dV$$

- The total viscous dissipation (**visc\_diss**)

$$\langle \Phi \rangle = \int \Phi dV = \frac{1}{V} \int 2\eta \dot{\epsilon} : \dot{\epsilon} dV$$

- The gravitational potential energy (**EG**)

$$E_G = \int_V \rho g_y (L_y - y) dV$$

- The internal thermal energy (**ET**)

$$E_T = \int_V \rho_{(0)} C_p T dV$$

**Remark 3:** Measuring the total mass can be misleading: indeed because  $\rho = \rho_0(1 - \alpha T)$ , then measuring the total mass amounts to measuring a constant minus the volume-integrated temperature, and there is no reason why the latter should be zero, so that there is no reason why the total mass should be zero...!

### 23.3 The experimental setup

The setup is as follows: the domain is  $Lx = Ly = 3000\text{km}$ . Free slip boundary conditions are imposed on all four sides. The initial temperature is given by:

$$T(x, y) = \left( \frac{L_y - y}{Ly} - 0.01 \cos\left(\frac{\pi x}{L_x}\right) \sin\left(\frac{\pi y}{Ly}\right) \right) \Delta T + T_{surf}$$

with  $\Delta T = 4000\text{K}$ ,  $T_{surf} = T_0 = 273.15\text{K}$ . The temperature is set to  $\Delta T + T_{surf}$  at the bottom and  $T_{surf}$  at the top. We also set  $k = 3$ ,  $C_p = 1250$ ,  $|g| = 10$ ,  $\rho_0 = 3000$  and we keep the Rayleigh number  $Ra$  and dissipation number  $Di$  as input parameters:

$$Ra = \frac{\alpha g \Delta T L^3 \rho_0^2 C_p}{\eta k} \quad Di = \frac{\alpha g L}{C_p}$$

From the second equation we get  $\alpha = \frac{DiC_p}{gL}$ , which we can insert in the first one:

$$Ra = \frac{DiC_p^2 \Delta T L^2 \rho_0^2}{\eta k} \quad \text{or,} \quad \eta = \frac{DiC_p^2 \Delta T L^2 \rho_0^2}{Ra k}$$

For instance, for  $Ra = 10^4$  and  $Di = 0.75$ , we obtain  $\alpha \simeq 3 \cdot 10^{-5}$  and  $\eta \simeq 10^{25}$  which are quite reasonable values.

## 23.4 Scaling

Following [31], we non-dimensionalize the equations using the reference values for density  $\rho_r$ , thermal expansivity  $\alpha_r$ , temperature contrast  $\Delta T_r$  (`refTemp`), thermal conductivity  $k_r$ , heat capacity  $C_p$ , depth of the fluid layer  $L$  and viscosity  $\eta_r$ . The non-dimensionalization for velocity,  $u_r$ , pressure  $p_r$  and time,  $t_r$  become

$$u_r = \frac{k_r}{\rho_r C_p L} \quad (\text{refvel})$$

$$p_r = \frac{\eta_r k_r}{\rho_r C_p L^2} \quad (\text{refpress})$$

$$t_r = \frac{\rho_r C_p L^2}{k_r} \quad (\text{reftime})$$

In the case of the setup described hereabove, and when choosing  $Ra = 10^4$  and  $Di = 0.5$ , we get:

```
alphaT 2.083333e-05
eta 8.437500e+24
reftime 1.125000e+19
refvel 2.666667e-13
refPress 7.500000e+05
```

## 23.5 Conservation of energy 1

### 23.5.1 under BA and EBA approximations

Following [33], we take the dot product of the momentum equation with the velocity  $\mathbf{v}$  and integrate over the whole volume<sup>4</sup>:

$$\int_V [-\nabla \cdot \boldsymbol{\tau} + \nabla p] \cdot \mathbf{v} dV = \int_V \rho \mathbf{g} \cdot \mathbf{v} dV$$

or,

$$-\int_V (\nabla \cdot \boldsymbol{\tau}) \cdot \mathbf{v} dV + \int_V \nabla p \cdot \mathbf{v} dV = \int_V \rho \mathbf{g} \cdot \mathbf{v} dV$$

Let us look at each block separately:

$$-\int_V (\nabla \cdot \boldsymbol{\tau}) \cdot \mathbf{v} dV = -\int_S \underbrace{\boldsymbol{\tau} \cdot \mathbf{n}}_{=0 \text{ (b.c.)}} dS + \int_V \boldsymbol{\tau} : \nabla \mathbf{v} dV = \int_V \boldsymbol{\tau} : \dot{\boldsymbol{\epsilon}} dV = \int_V \Phi dV$$

which is the volume integral of the shear heating. Then,

$$\int_V \nabla p \cdot \mathbf{v} dV = \int_S \underbrace{p \cdot \mathbf{n}}_{=0 \text{ (b.c.)}} dS - \int_V \underbrace{\nabla \cdot \mathbf{v}}_{=0 \text{ (incomp.)}} pdV = 0$$

which is then zero in the case of an incompressible flow. And finally

$$\int_V \rho \mathbf{g} \cdot \mathbf{v} dV = W$$

which is the work against gravity.

Conclusion for an *incompressible* fluid: we should have

$$\int_V \Phi dV = \int_V \rho \mathbf{g} \cdot \mathbf{v} dV \tag{90}$$

---

<sup>4</sup>Check: this is akin to looking at the power, force\*velocity, says Arie

This formula is hugely problematic: indeed, the term  $\rho$  in the rhs is the full density. We know that to the value of  $\rho_0$  corresponds a lithostatic pressure gradient  $p_L = \rho_0 gy$ . In this case one can write  $\rho = \rho_0 + \rho'$  and  $p = p_L + p'$  so that we also have

$$\int_V [-\nabla \cdot \boldsymbol{\tau} + \nabla p'] \cdot \mathbf{v} dV = \int_V \rho' \mathbf{g} \cdot \mathbf{v} dV$$

which will ultimately yield

$$\int_V \Phi dV = \int_V \rho' \mathbf{g} \cdot \mathbf{v} dV = \int_V (\rho - \rho_0) \mathbf{g} \cdot \mathbf{v} dV \quad (91)$$

Obviously Eqs.(90) and (91) cannot be true at the same time. The problem comes from the nature of the (E)BA approximation:  $\rho = \rho_0$  in the mass conservation equation but it is not constant in the momentum conservation equation, which is of course inconsistent. Since the mass conservation equation is  $\nabla \cdot \mathbf{v} = 0$  under this approximation then the term  $\int_V \nabla p \cdot \mathbf{v} dV$  is always zero for any pressure (full pressure  $p$ , or overpressure  $p - p_L$ ), hence the paradox. This paradox will be lifted when a consistent set of equations will be used (compressible formulation). On a practical note, Eqs.(90) is not verified by the code, while (91) is.

In the end:

$$\boxed{\underbrace{\int_V \Phi dV}_{\text{visc\_diss}} = \underbrace{\int_V (\rho - \rho_0) \mathbf{g} \cdot \mathbf{v} dV}_{\text{work\_grav}}} \quad (92)$$

### 23.5.2 under no approximation at all

$$\int_V \nabla p \cdot \mathbf{v} dV = \int_S \underbrace{p \cdot \mathbf{n}}_{=0 \text{ (b.c.)}} dS - \int_V \nabla \cdot \mathbf{v} p dV = 0 \quad (93)$$

$$= \int_V \frac{1}{\rho} \mathbf{v} \cdot \nabla \rho p dV = 0 \quad (94)$$

(95)

**ToDo:** see section 3 of [33] where this is carried out with the Adams-Williamson eos.

## 23.6 Conservation of energy 2

Also, following the Reynold's transport theorem [37], p210, we have for a property  $A$  (per unit mass)

$$\frac{d}{dt} \int_V A \rho dV = \int_V \frac{\partial}{\partial t} (A \rho) dV + \int_S A \rho \mathbf{v} \cdot \mathbf{n} dS$$

Let us apply to this to  $A = C_p T$  and compute the time derivative of the internal energy:

$$\frac{d}{dt} \int_V \rho C_p T dV = \int_V \frac{\partial}{\partial t} (\rho C_p T) dV + \int_S \underbrace{A \rho \cdot \mathbf{n}}_{=0 \text{ (b.c.)}} dS = \underbrace{\int_V C_p T \frac{\partial \rho}{\partial t} dV}_I + \underbrace{\int_V \rho C_p \frac{\partial T}{\partial t} dV}_{II} \quad (96)$$

In order to expand  $I$ , the mass conservation equation will be used, while the heat transport equation will be used for  $II$ :

$$I = \int_V C_p T \frac{\partial \rho}{\partial t} dV = - \int_V C_p T \nabla \cdot (\rho \mathbf{v}) dV = - \int_V C_p T \rho \underbrace{\mathbf{v} \cdot \mathbf{n}}_{=0 \text{ (b.c.)}} dS + \int_V \rho C_p \nabla T \cdot \mathbf{v} dV \quad (97)$$

$$II = \int_V \rho C_p \frac{\partial T}{\partial t} dV = \int_V \left[ -\rho C_p \mathbf{v} \cdot \nabla T + \nabla \cdot k \nabla T + \rho H + \Phi + \alpha T \left( \frac{\partial p}{\partial t} + \mathbf{v} \cdot \nabla p \right) \right] dV \quad (98)$$

$$= \int_V \left[ -\rho C_p \mathbf{v} \cdot \nabla T + \rho H + \Phi + \alpha T \left( \frac{\partial p}{\partial t} + \mathbf{v} \cdot \nabla p \right) \right] dV + \int_V \nabla \cdot k \nabla T dV \quad (99)$$

$$= \int_V \left[ -\rho C_p \mathbf{v} \cdot \nabla T + \rho H + \Phi + \alpha T \left( \frac{\partial p}{\partial t} + \mathbf{v} \cdot \nabla p \right) \right] dV + \int_S k \nabla T \cdot \mathbf{n} dS \quad (100)$$

$$= \int_V \left[ -\rho C_p \mathbf{v} \cdot \nabla T + \rho H + \Phi + \alpha T \left( \frac{\partial p}{\partial t} + \mathbf{v} \cdot \nabla p \right) \right] dV - \int_S \mathbf{q} \cdot \mathbf{n} dS \quad (101)$$

Finally:

$$I + II = \underbrace{\frac{d}{dt} \int_V \rho C_p T dV}_{ET} = \int_V \left[ \rho H + \Phi + \alpha T \left( \frac{\partial p}{\partial t} + \mathbf{v} \cdot \nabla p \right) \right] dV - \int_S \mathbf{q} \cdot \mathbf{n} dS \quad (102)$$

$$= \underbrace{\int_V \rho H dV}_{visc\_diss} + \underbrace{\int_V \alpha T \frac{\partial p}{\partial t} dV}_{extra} + \underbrace{\int_V \alpha T \mathbf{v} \cdot \nabla p dV}_{adiab\_heating} - \underbrace{\int_S \mathbf{q} \cdot \mathbf{n} dS}_{heatflux\_boundary} \quad (103)$$

This was of course needlessly complicated as the term  $\partial \rho / \partial t$  is always taken to be zero, so that  $I = 0$  automatically. The mass conservation equation is then simply  $\nabla \cdot (\rho \mathbf{v}) = 0$ . Then it follows that

$$0 = \int_V C_p T \nabla \cdot (\rho \mathbf{v}) dV = - \int_V C_p T \rho \underbrace{\mathbf{v} \cdot \mathbf{n}}_{=0 \text{ (b.c.)}} dS + \int_V \rho C_p \nabla T \cdot \mathbf{v} dV \quad (104)$$

$$= \int_V \rho C_p \nabla T \cdot \mathbf{v} dV \quad (105)$$

so that the same term in Eq.(101) vanishes too, and then Eq.(103) is always valid, although one should be careful when computing  $E_T$  in the BA and EBA cases as it should use  $\rho_0$  and not  $\rho$ .

### 23.7 The problem of the onset of convection

[wiki] In geophysics, the Rayleigh number is of fundamental importance: it indicates the presence and strength of convection within a fluid body such as the Earth's mantle. The mantle is a solid that behaves as a fluid over geological time scales.

The Rayleigh number essentially is an indicator of the type of heat transport mechanism. At low Rayleigh numbers conduction processes dominate over convection ones. At high Rayleigh numbers it is the other way around. There is a so-called critical value of the number with delineates the transition from one regime to the other.

This problem has been studied and approached both theoretically and numerically [55, e.g.] and it was found that the critical Rayleigh number  $Ra_c$  is

$$Ra_c = (27/4)\pi^4 \simeq 657.5$$

in setups similar to ours.

#### VERY BIG PROBLEM

The temperature setup is built as follows:  $T_{surf}$  is prescribed at the top,  $T_{surf} + \Delta T$  is prescribed at the bottom. The initial temperature profile is linear between these two values. In the case of BA, the actual value of  $T_{surf}$  is of no consequence. However, for the EBA the full temperature is present in the adiabatic heating term on the rhs of the hte, and the value of  $T_{surf}$  will therefore influence the solution greatly. This is very problematic as there is no real way to arrive at the surface temperature from the King paper. On top of this, the density uses a reference temperature  $T_0$  which too will influence the solution without being present in the controlling  $Ra$  and  $Di$  numbers!!

In light thereof, it will be very difficult to recover the values of King et al for EBA!

## features

- $Q_1 \times P_0$  element
- compressible flow
- mixed formulation
- Dirichlet boundary conditions (no-slip)
- isoviscous
- analytical solution
- pressure smoothing

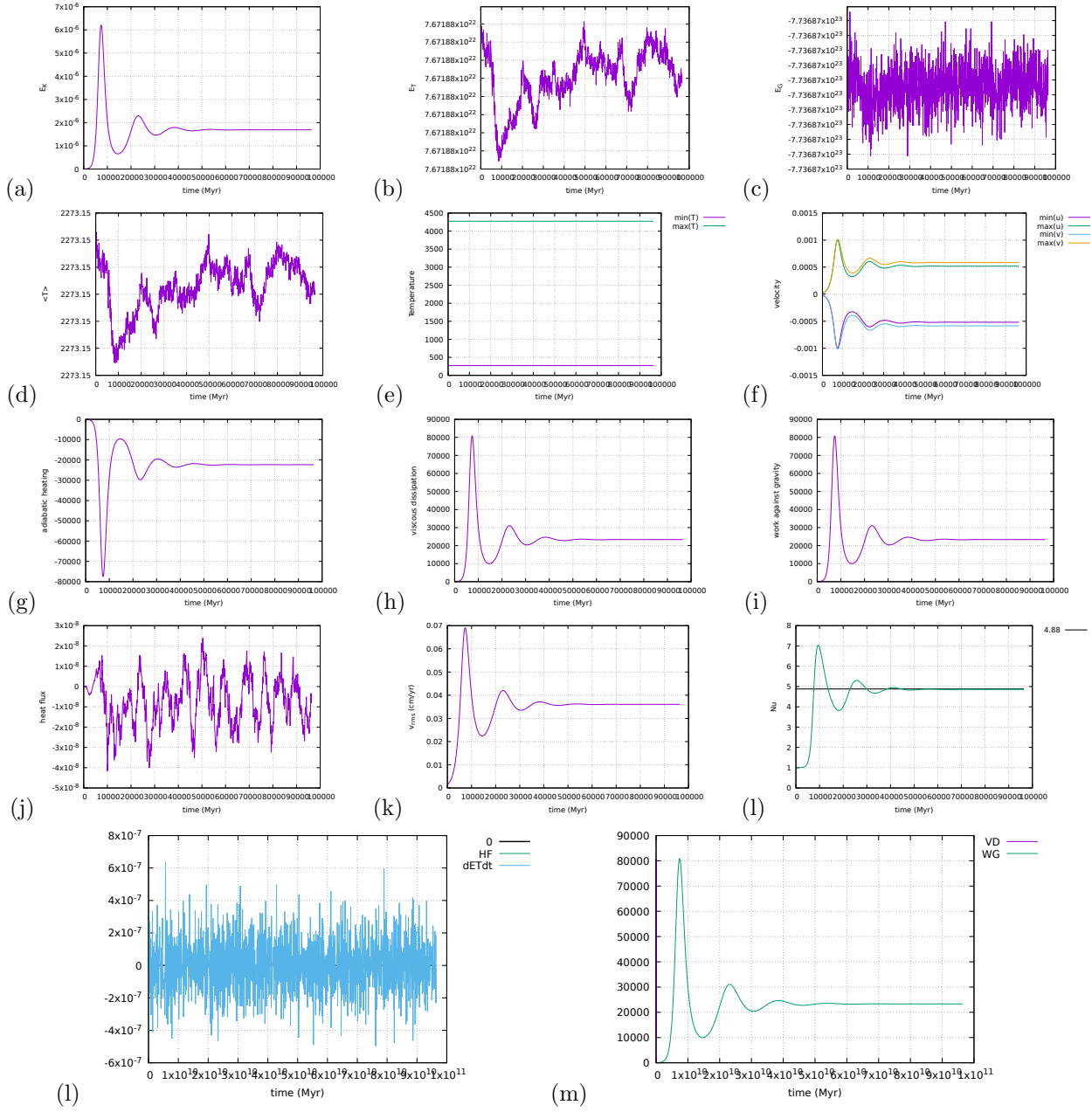
Relevant literature: [4, 28, 50, 33, 31, 34, 35, 24]

ToDo:

- heat flux is at the moment elemental, so Nusselt and heat flux on boundaries measurements not as accurate as could be.
- implement steady state detection
- do  $Ra = 10^5$  and  $Ra = 10^6$
- velocity average at surface
- non dimensional heat flux at corners [5]
- depth-dependent viscosity (case 2 of [5])

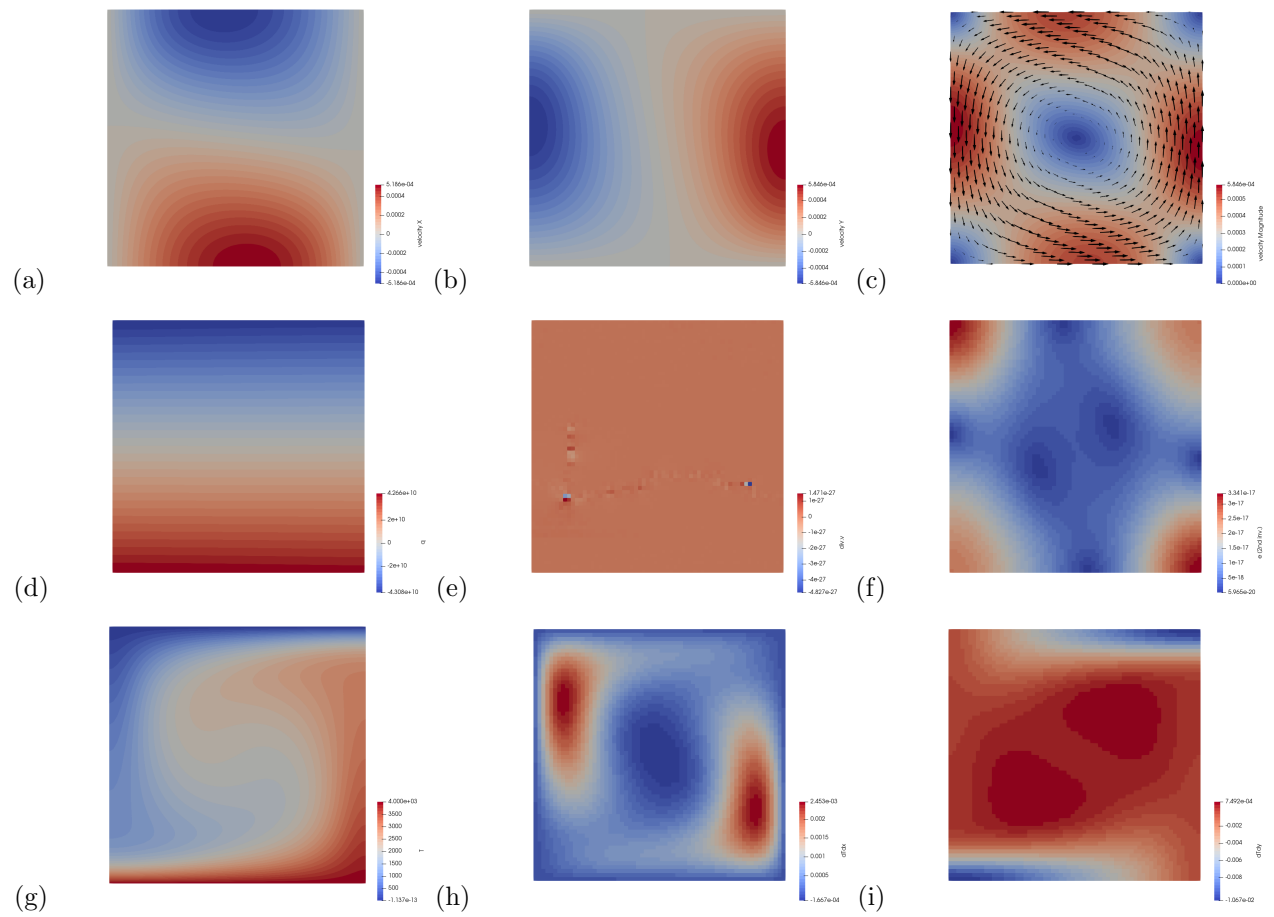
## 23.8 results - BA - $Ra = 10^4$

These results were obtained with a 64x64 resolution, and CFL number of 1. Steady state was reached after about 1250 timesteps.



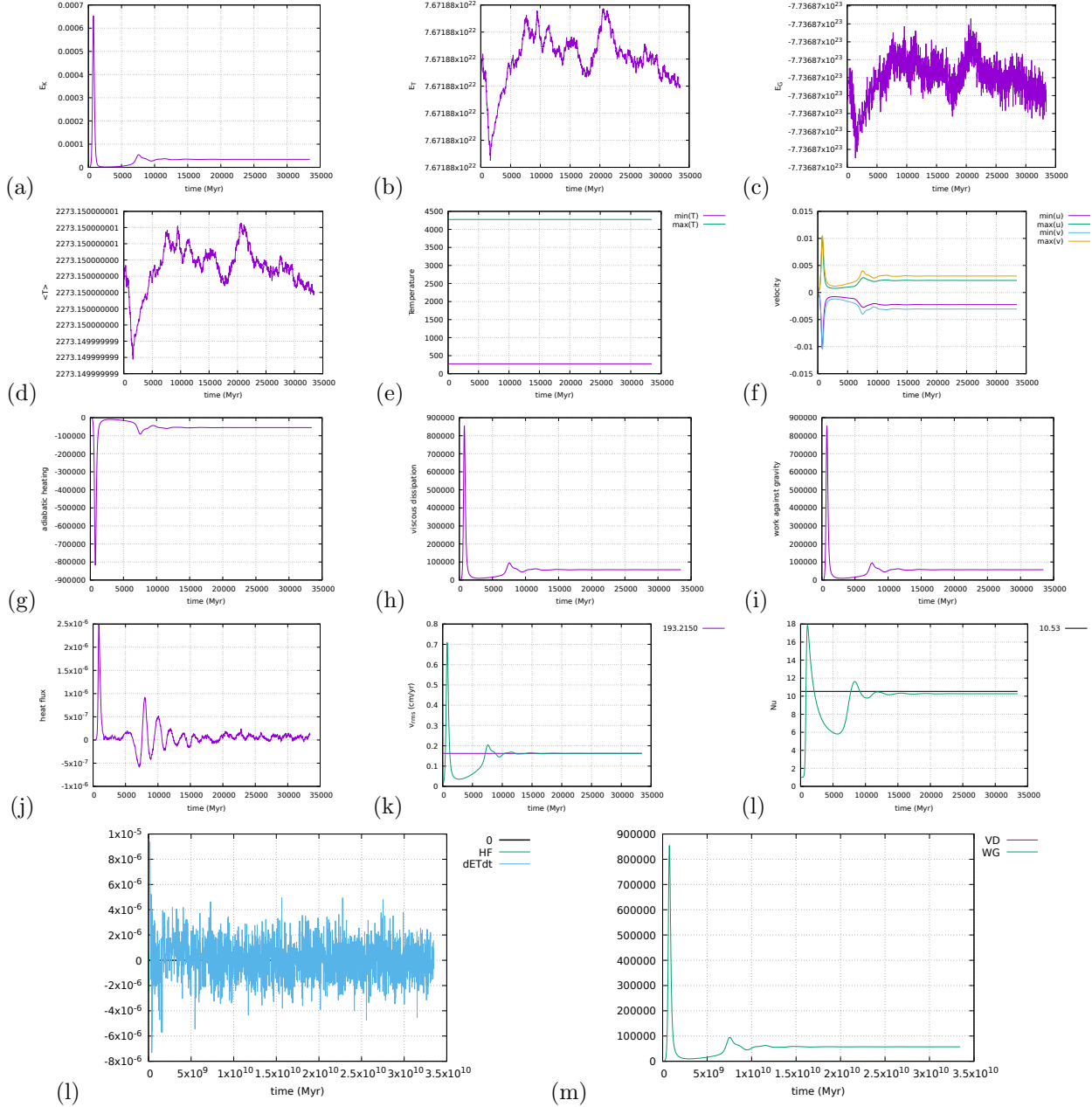
AH: adiabatic heating, VD: viscous dissipation, HF: heat flux, WG: work against gravity

Eq.(103) is verified by (l) and Eq.(92) is verified by (m).



### 23.9 results - BA - $Ra = 10^5$

These results were obtained with a 64x64 resolution, and CFL number of 1. Steady state was reached after about 1250 timesteps.

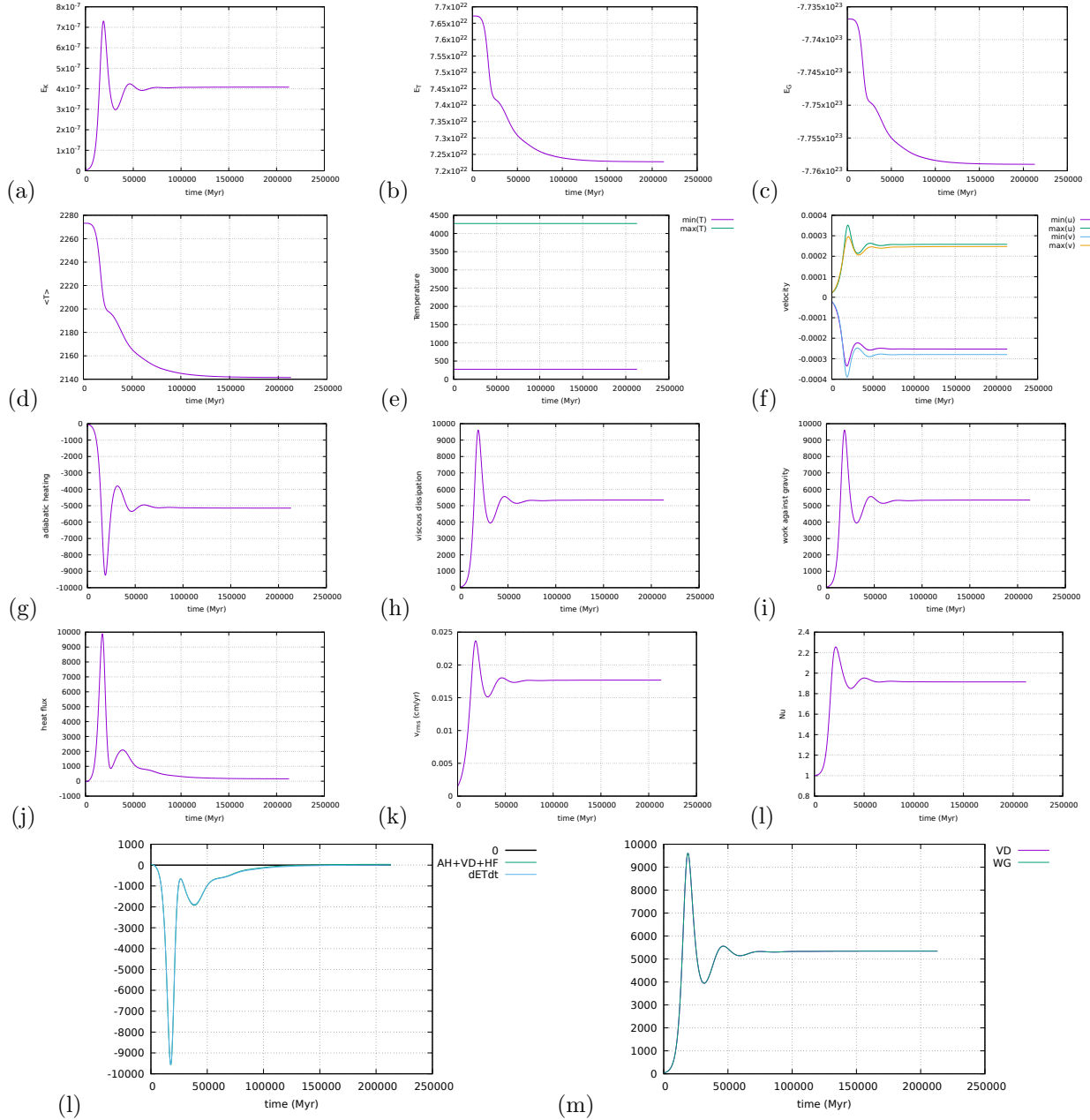


Eq.(103) is verified by (l) and Eq.(92) is verified by (m).

## **23.10 results - BA - $Ra = 10^6$**

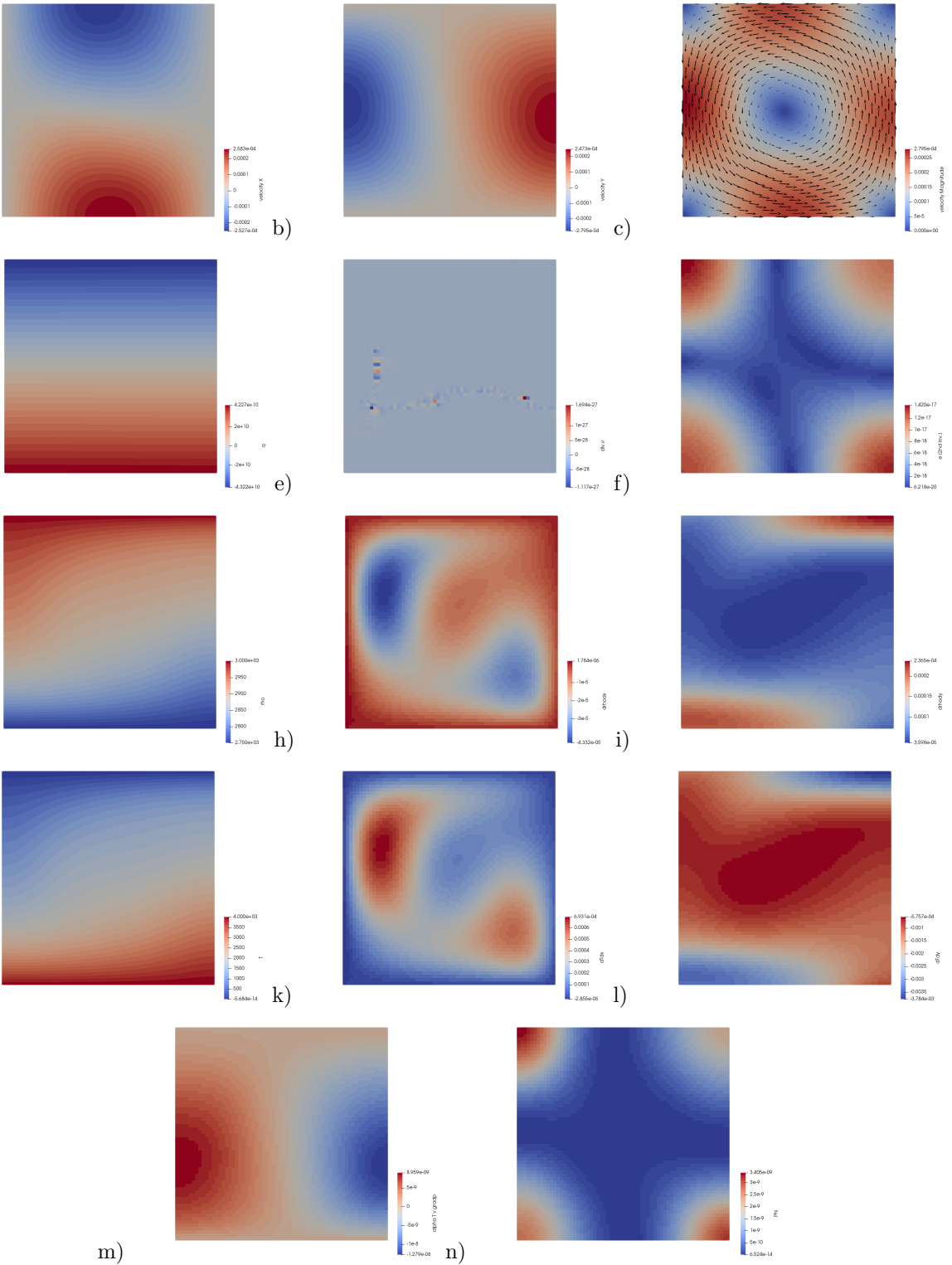
### 23.11 results - EBA - $Ra = 10^4$

These results were obtained with a 64x64 resolution, and CFL number of 1. Steady state was reached after about 2500 timesteps



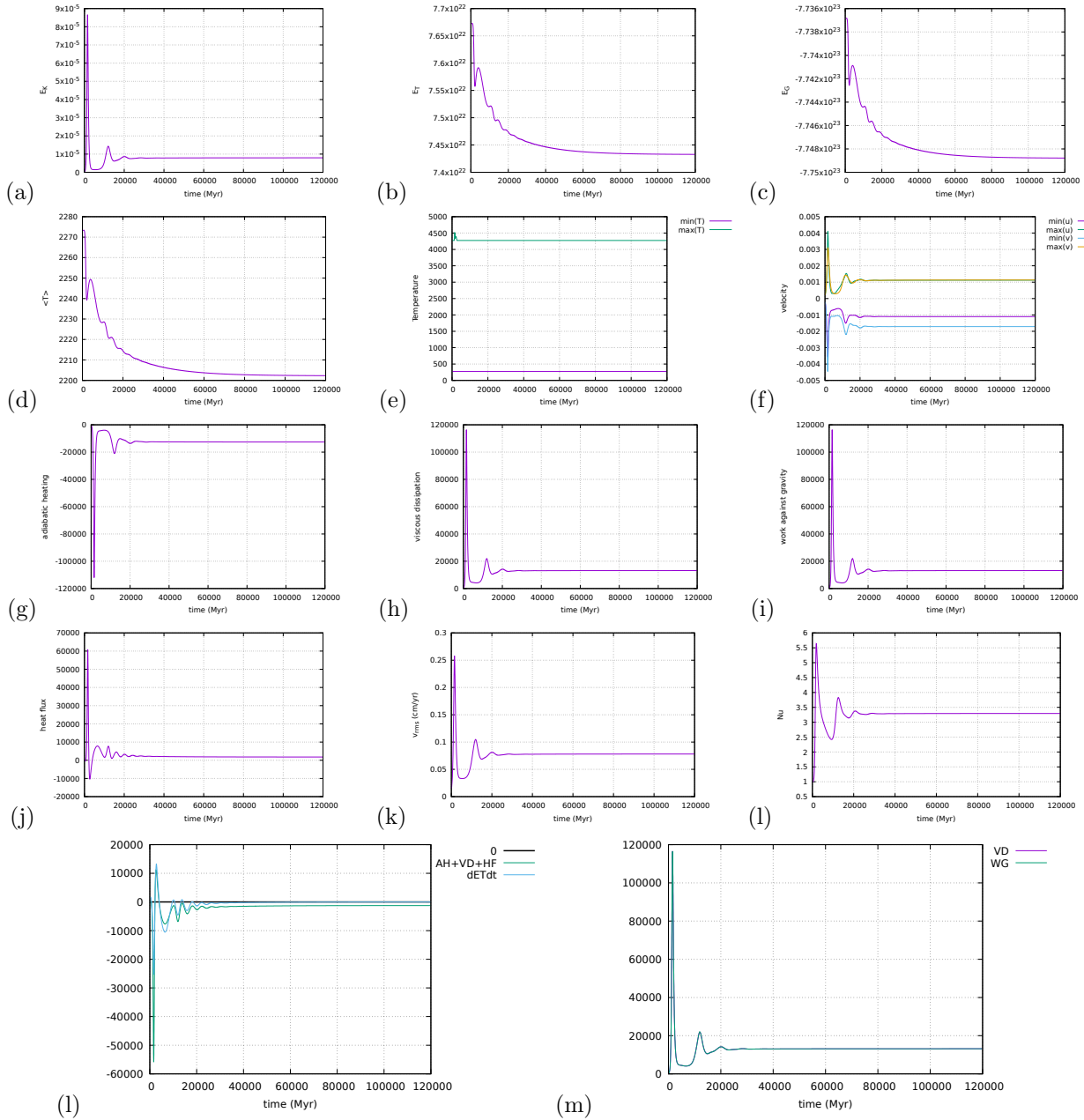
AH: adiabatic heating, VD: viscous dissipation, HF: heat flux, WG: work against gravity

Eq.(103) is verified by (l) and Eq.(92) is verified by (m).



## 23.12 results - EBA - $Ra = 10^5$

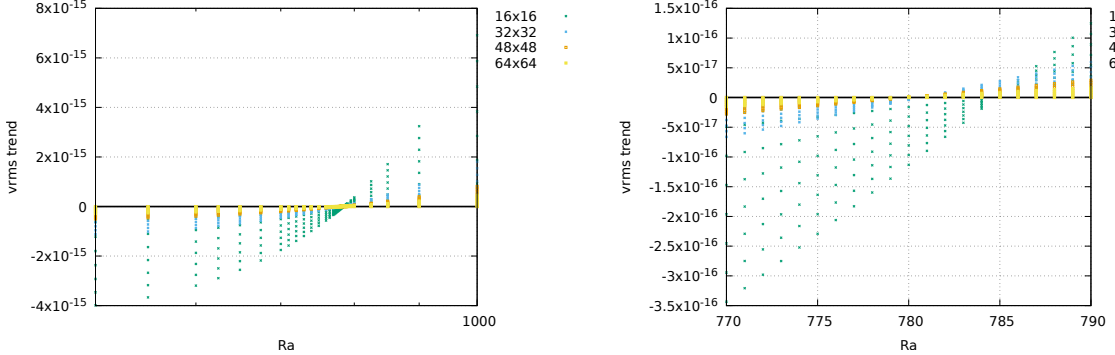
These results were obtained with a 64x64 resolution, and CFL number of 1. Simulation was stopped after about 4300 timesteps.



AH: adiabatic heating, VD: viscous dissipation, HF: heat flux, WG: work against gravity

### 23.13 Onset of convection

The code can be run for values of  $\text{Ra}$  between 500 and 1000, at various resolutions for the BA formulation. The value  $v_{rms}(t) - v_{rms}(0)$  is plotted as a function of  $\text{Ra}$  and for the 10 first timesteps. If the  $v_{rms}$  is found to decrease, then the Rayleigh number is not high enough to allow for convection and the initial temperature perturbation relaxes by diffusion (and then  $v_{rms}(t) - v_{rms}(0) < 0$ ). If the  $v_{rms}$  is found to increase, then  $v_{rms}(t) - v_{rms}(0) > 0$  and the system is going to showcase convection. The zero value of  $v_{rms}(t) - v_{rms}(0)$  gives us the critical Rayleigh number, which is found between 775 and 790.



## A The main codes in computational geodynamics

In what follows I make a quick inventory of the main codes of computational geodynamics, for crust, lithosphere and/or mantle modelling.

**A.1 ADELI**

**A.2 ASPECT**

**A.3 CITCOMS and CITCOMCU**

**A.4 DOUAR**

**A.5 GAIA**

**A.6 GALE**

**A.7 GTECTON**

**A.8 ELVIS**

**A.9 ELEFANT**

**A.10 ELLIPSIS**

**A.11 FANTOM**

**A.12 FLUIDITY**

**A.13 LAMEM**

**A.14 MILAMIN**

**A.15 PARAVOZ/FLAMAR**

**A.16 PTATIN**

**A.17 RHEA**

**A.18 SEPRAN**

**A.19 SOPALE**

**A.20 STAGYY**

**A.21 SULEC**

SULEC is a finite element code that solves the incompressible Navier-Stokes equations for slow creeping flows. The code is developed by Susan Ellis (GNS Sciences, NZ) and Susanne Buitter (NGU).

**A.22 TERRA**

**A.23 UNDERWORLD 1&2**

## B fieldstone.py

- C fieldstone\_stokes\_sphere.py
- D fieldstone\_convection\_box.py

## E fieldstone\_solcx.py

## F fieldstone\_indentor.py

## G fieldstone\_saddlepoint.py

## References

- [1] M. Albers. A local mesh refinement multigrid method for 3D convection problems with strongly variable viscosity. *J. Comp. Phys.*, 160:126–150, 2000.
- [2] K.-J. Bathe. *Finite Element Procedures in Engineering Analysis*. Prentice-Hall, 1982.
- [3] M. Benzi, G.H. Golub, and J. Liesen. Numerical solution of saddle point problems. *Acta Numerica*, 14:1–137, 2005.
- [4] D. Bercovici, G. Schubert, and G.A. Glatzmaier. Three-dimensional convection of an infinite Prandtl-number compressible fluid in a basally heated spherical shell. *J. Fluid Mech.*, 239:683–719, 1992.
- [5] B. Blankenbach, F. Busse, U. Christensen, L. Cserepes, D. Gunkel, U. Hansen, H. Harder, G. Jarvis, M. Koch, G. Marquart, D. Moore, P. Olson, H. Schmeling, and T. Schnaubelt. A benchmark comparison for mantle convection codes. *Geophys. J. Int.*, 98:23–38, 1989.
- [6] H.H. Bui, R. Fukugawa, K. Sako, and S. Ohno. Lagrangian meshfree particles method (SPH) for large deformation and failure flows of geomaterial using elasticplastic soil constitutive model. *Int. J. Numer. Anal. Geomech.*, 32(12):1537–1570, 2008.
- [7] C. Burstedde, G. Stadler, L. Alisic, L.C. Wilcox, E. Tan, M. Gurnis, and O. Ghattas. Large-scale adaptive mantle convection simulation. *Geophys. J. Int.*, 192:889–906, 2013.
- [8] Edmund Christiansen and Knud D. Andersen. Computation of collapse states with von mises type yield condition. *International Journal for Numerical Methods in Engineering*, 46:1185–1202, 1999.
- [9] Edmund Christiansen and Ole S. Pedersen. Automatic mesh refinement in limit analysis. *International Journal for Numerical Methods in Engineering*, 50:1331–1346, 2001.
- [10] C. Cuvelier, A. Segal, and A.A. van Steenhoven. *Finite Element Methods and Navier-Stokes Equations*. D. Reidel Publishing Company, 1986.
- [11] D.R. Davies, C.R. Wilson, and S.C. Kramer. Fluidity: A fully unstructured anisotropic adaptive mesh computational modeling framework for geodynamics. *Geochem. Geophys. Geosyst.*, 12(6), 2011.
- [12] P. Davy and P. Cobbold. Indentation tectonics in nature and experiment. 1. experiments scaled for gravity. *Bulletin of the Geological Institutions of Uppsala*, 14:129–141, 1988.
- [13] Y. Deubelbeiss and B.J.P. Kaus. Comparison of Eulerian and Lagrangian numerical techniques for the Stokes equations in the presence of strongly varying viscosity. *Phys. Earth Planet. Interiors*, 171:92–111, 2008.
- [14] C.R. Dohrmann and P.B. Bochev. A stabilized finite element method for the Stokes problem based on polynomial pressure projections. *Int. J. Num. Meth. Fluids*, 46:183–201, 2004.
- [15] J. Donea and A. Huerta. *Finite Element Methods for Flow Problems*. 2003.
- [16] J. Donea and A. Huerta. *Finite Element Methods for Flow Problems*. John Wiley & Sons, 2003.
- [17] Jean Donea and Antonio Huerta. *Finite Element Methods for Flow Problems*. John Wiley & Sons, 2003.
- [18] T. Duretz, D.A. May, T.V. Gerya, and P.J. Tackley. Discretization errors and free surface stabilisation in the finite difference and marker-in-cell method for applied geodynamics: A numerical study. *Geochem. Geophys. Geosyst.*, 12(Q07004), 2011.
- [19] M. Gerbault, A.N.B. Poliakov, and M. Daignieres. Prediction of faulting from the theories of elasticity and plasticity: what are the limits? *Journal of Structural Geology*, 20:301–320, 1998.
- [20] Taras Gerya. *Numerical Geodynamic Modelling*. Cambridge University Press, 2010.
- [21] T.V. Gerya, D.A. May, and T. Duretz. An adaptive staggered grid finite difference method for modeling geodynamic Stokes flows with strongly variable viscosity. *Geochem. Geophys. Geosyst.*, 14(4), 2013.
- [22] G.H. Golub and C.F. van Loan. *Matrix Computations, 4th edition*. John Hopkins University Press, 2013.
- [23] M. Gunzburger. *Finite Element Methods for Viscous Incompressible Flows: A Guide to Theory, Practice and Algorithms*. Academic, Boston, 1989.

- [24] T. Heister, J. Dannberg, R. Gassmöller, and W. Bangerth. High Accuracy Mantle Convection Simulation through Modern Numerical Methods. II: Realistic Models and Problems. *Geophys. J. Int.*, 210(2):833–851, 2017.
- [25] T.J.R. Hughes. *The Finite Element Method. Linear Static and Dynamic Finite Element Analysis*. Dover Publications, Inc., 2000.
- [26] T.J.R. Hughes, W.K. Liu, and A. Brooks. Finite element analysis of Incompressible viscous flows by the penalty function formulation. *J. Comp. Phys.*, 30:1–60, 1979.
- [27] Hoon Huh, Choong Ho Lee, and Wei H. Yang. A general algorithm for plastic flow simulation by finite element limit analysis. *International Journal of Solids and Structures*, 36:1193–1207, 1999.
- [28] J. Ita and S.D. King. Sensitivity of convection with an endothermic phase change to the form of governing equations, initial conditions, boundary conditions, and equation of state. *J. Geophys. Res.*, 99(B8):15,919–15,938, 1994.
- [29] L. Jolivet, P. Davy, and P. Cobbold. Right-lateral shear along the Northwest Pacific margin and the India-Eurasia collision. *Tectonics*, 9(6):1409–1419, 1990.
- [30] L.M. Kachanov. *Fundamentals of the Theory of Plasticity*. Dover Publications, Inc., 2004.
- [31] S. King, C. Lee, P. van Keken, W. Leng, S. Zhong, E. Tan, N. Tosi, and M. Kameyama. A community benchmark for 2D Cartesian compressible convection in the Earths mantle. *Geophys. J. Int.*, 180:7387, 2010.
- [32] M. Kronbichler, T. Heister, and W. Bangerth. High accuracy mantle convection simulation through modern numerical methods . *Geophys. J. Int.*, 191:12–29, 2012.
- [33] W. Leng and S. Zhong. Viscous heating, adiabatic heating and energetic consistency in compressible mantle convection. *Geophys. J. Int.*, 173:693–702, 2008.
- [34] W. Leng and S. Zhong. Implementation and application of adaptive mesh refinement for thermochemical mantle convection studies. *Geochem. Geophys. Geosyst.*, 12(4), 2011.
- [35] X. Liu and S. Zhong. Analyses of marginal stability, heat transfer and boundary layer properties for thermal convection in a compressible fluid with infinite Prandtl number. *Geophys. J. Int.*, 194:125–144, 2013.
- [36] D.S. Malkus and T.J.R. Hughes. Mixed finite element methods - reduced and selective integration techniques: a unification of concepts. *Comput. Meth. Appl. Mech. Eng.*, 15:63–81, 1978.
- [37] L.E. Malvern. *Introduction to the mechanics of a continuous medium*. Prentice-Hall, Inc., 1969.
- [38] P. Molnar and P. Tapponnier. Relation of the tectonics of eastern China to the India-Eurasia collision: Application of the slip-line field theory to large-scale continental tectonics. *Geology*, 5:212–216, 1977.
- [39] L. Moresi, S. Quenette, V. Lemiale, C. Mériaux, B. Appelbe, and H.-B. Mühlhaus. Computational approaches to studying non-linear dynamics of the crust and mantle. *Phys. Earth. Planet. Inter.*, 163:69–82, 2007.
- [40] G. Peltzer and P. Tapponnier. Formation and evolution of strike-slip faults, rifts, and basins during the india-asia collision: an experimental approach. *J. Geophys. Res.*, 93(B12):15085–15177, 1988.
- [41] A.E. Pusok, B.J.P. Kaus, and A.A. Popov. On the Quality of Velocity Interpolation Schemes for Marker-in-Cell Method and Staggered Grids. *Pure and Applied Geophysics*, pages doi:10.1007/s00024-016-1431-8, 2016.
- [42] T. Rabczuk, P.M.A. Areias, and T. Belytschko. A simplified mesh-free method for shear bands with cohesive surfaces . *Int. J. Num. Meth. Eng.*, 69:993–1021, 2007.
- [43] J.N. Reddy. On penalty function methods in the finite element analysis of flow problems. *Int. J. Num. Meth. Fluids*, 2:151–171, 1982.
- [44] J. Revenaugh and B. Parsons. Dynamic topography and gravity anomalies for fluid layers whose viscosity varies exponentially with depth. *Geophysical Journal of the Royal Astronomical Society*, 90(2):349–368, 1987.
- [45] H. Schmeling, A.Y. Babeyko, A. Enns, C. Faccenna, F. Funiciello, T. Gerya, G.J. Golabek, S. Grigull, B.J.P. Kaus, G. Morra, S.M. Schmalholz, and J. van Hunen. A benchmark comparison of spontaneous subduction models - Towards a free surface. *Phys. Earth. Planet. Inter.*, 171:198–223, 2008.
- [46] D.W. Schmid and Y.Y. Podlachikov. Analytical solutions for deformable elliptical inclusions in general shear. *Geophys. J. Int.*, 155:269–288, 2003.

- [47] G. Schubert, D.L. Turcotte, and P. Olson. *Mantle Convection in the Earth and Planets*. Cambridge University Press, 2001.
- [48] J. Suckale, J.-C. Nave, and B.H. Hager. It takes three to tango: 1. Simulating buoyancy-driven flow in the presence of large viscosity contrasts. *J. Geophys. Res.*, 115(B07409), 2010.
- [49] P. Tackley. *Three-dimensional models of mantle convection: Influence of phase transitions and temperature-dependent viscosity*. PhD thesis, California Institute of Technology, 1994.
- [50] E. Tan and M. Gurnis. Compressible thermochemical convection and application to lower mantle structures. *J. Geophys. Res.*, 112(B06304), 2007.
- [51] Paul Tapponnier and Peter Molnar. Slip-line field theory and large-scale continental tectonics. *Nature*, 264:319–324, November 1976.
- [52] M. Thielmann, D.A. May, and B.J.P. Kaus. Discretization errors in the Hybrid Finite Element Particle-In-Cell Method. *Pure and Applied Geophysics*, 2014.
- [53] C. Thieulot, P. Fullsack, and J. Braun. Adaptive octree-based finite element analysis of two- and three-dimensional indentation problems. *J. Geophys. Res.*, 113:B12207, 2008.
- [54] R.A. Trompert and U. Hansen. On the Rayleigh number dependence of convection with a strongly temperature-dependent viscosity. *Physics of Fluids*, 10(2):351–360, 1998.
- [55] D.L. Turcotte and G. Schubert. *Geodynamics, 2nd edition*. Cambridge, 2012.
- [56] X. Yu and F. Tin-Loi. A simple mixed finite element for static limit analysis. *Computers and Structures*, 84:1906–1917, 2006.
- [57] S. Zhong. Analytic solutions for Stokes flow with lateral variations in viscosity. *Geophys. J. Int.*, 124:18–28, 1996.
- [58] O. Zienkiewicz and S. Nakazawa. The penalty function method and its application to the numerical solution of boundary value problems. *The American Society of Mechanical Engineers*, 51, 1982.
- [59] O.C. Zienkiewicz, M. Huang, and M. Pastor. Localization problems in plasticity using finite elements with adaptive remeshing. *International Journal for Numerical and Analytical Methods in Geomechanics*, 19:127–148, 1995.
- [60] O.C. Zienkiewicz, C. Humpheson, and R.W. Lewis. Associated and non-associated visco-plasticity and plasticity in soil mechanics . *Géotechnique*, 25(4):671–689, 1975.

# Index

$Q_1 \times P_0$ , 20, 26, 32, 38, 41, 51, 57  
 $Q_2 \times Q_1$ , 46

analytical solution, 20, 26, 41, 46, 48, 51, 57  
arithmetic mean, 38

basis functions, 12  
Boussinesq, 8  
bulk modulus, 52  
bulk viscosity, 5

compressibility, 52  
compressible flow, 57

dynamic viscosity, 5

Gauss quadrature, 10  
geometric mean, 38

harmonic mean, 38

incompressible flow, 26, 32, 38, 41, 46, 48, 51  
isothermal, 20, 26, 32, 38, 41, 46, 48, 51  
isoviscous, 20, 41, 46, 51, 57

Legendre polynomial, 10

midpoint rule, 9  
mixed formulation, 41, 46, 48, 51, 57

Newton-Cotes, 10  
non-isoviscous, 26, 32, 38, 48  
nonconforming  $Q_1 \times P_0$ , 48  
nonlinear rheology, 32

particle-in-cell, 38  
penalty formulation, 14, 20, 26, 32, 38  
pressure smoothing, 41, 48, 51, 57

quadrature, 10

rectangle rule, 9

second viscosity, 5

thermal expansion, 52  
trapezoidal rule, 9

weak form, 16  
work against gravity, 54